Stockholm University

Biomimetic Iron Complexes involved in Oxygenation and Chlorination

A Theoretical Study

Holger Noack

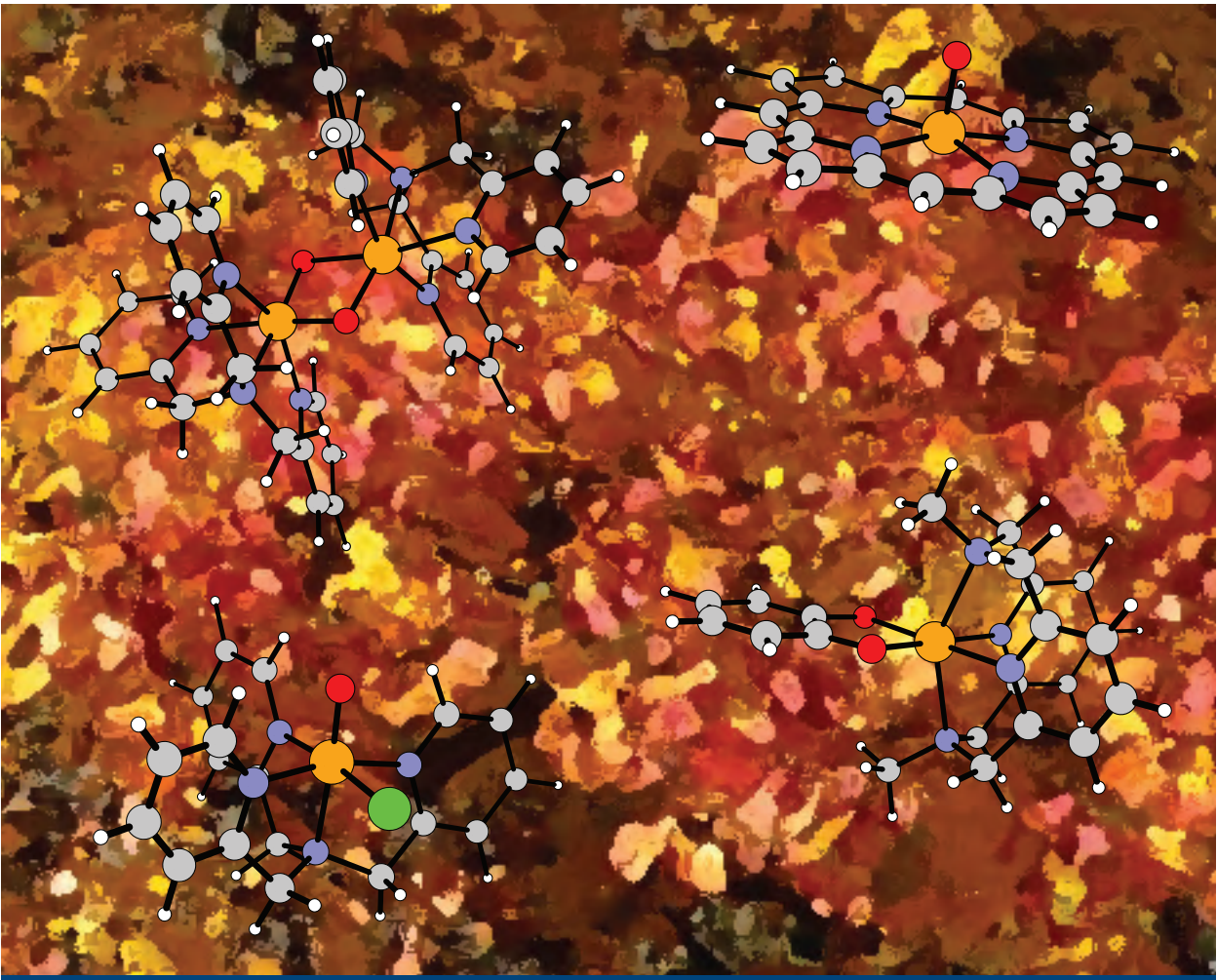

Doctoral Thesis in Chemical Physics at Stockholm University, Sweden 2010

Stockholm
University

Biomimetic Iron Complexes involved in Oxygenation and Chlorination

A Theoretical Study

Holger Noack

Dipl.-Chem. Holger Noack
Born 1976 in Berlin, Germany. Apprenticeship as Chemical Laboratory Worker at Fritz Haber Institute of the Max Planck Society, Berlin 1997–2000. Studies in Chemistry at Humboldt University, Berlin 2000–2005. PhD Studies in Chemical Physics at Stockholm University, Stockholm 2005–2010.

Thesis for the Degree of Doctor of Philosophy in Chemical Physics
Department of Physics
Stockholm University
Stockholm 2010

ISBN 978–91–7447–013–0
Printed by Universitetsservice US-AB, Stockholm

Pour mieux comprendre la chose
je vous conseille de lire tout le document.

Preface

This thesis is the result of my research years in the group of Margareta Blomberg and Per Siegbahn. My interest for chemistry began only after I finished secondary school, during my apprenticeship at the Fritz Haber Institute. One of my supervisors at that time, Olaf Timpe, enthused me for the subject with colorful reactions of heteropolyacids and exciting tales about chemistry. However, there was also the physicist Alexander Hahn. He repeatedly spoke to me about the importance of mathematics in every aspect of natural science, thereby glancing with some kind of mistrust at our laboratory equipment. Nonetheless, I felt inspired and it was a natural choice to study chemistry. But with time it became evident that Alexander had a point, not only because of the math exams one had to pass, but rather because all these formulas were actually needed to explain and handle certain aspects of chemistry. And so, the honorable quest to understand the picky questions slowly led away from the versatile lab life towards the rather tricky computer science, where all the quantum chemistry happens.

This is of course not everybody's avocation and most chemists react rather sceptic when it comes to theory. Therefore, I thought it might be of advantage to begin with a general introduction to the methodology that was applied in this thesis. In **chapter 1** the concepts of quantum chemistry and theoretical chemistry are presented in a way that allows the reader to get an idea of the methodology, hopefully without lowering the reading experience. The introduction continues in **chapter 2** where the chemical background to this thesis is provided, looking at the role of iron in biochemistry and biomimetic chemistry. Here the emphasis will be on those enzymes that are related to the work presented in the subsequent chapters.

The title of this thesis "Biomimetic Iron Complexes involved in Oxygenation and Chlorination" points out the two kind of reactions that are investigated. Oxygenation refers to a reaction in which oxygen is incorporated into the substrate, and similarly chlorination describes the incorporation of chlorine. Both kind of reactions have in common that they oxidize the organic substrate, and the oxidizing agent used throughout all

the reactions presented is dioxygen. Furthermore, most reactions start out with hydrogen atom abstraction from the substrate to the activated oxygen, which leads to the formation of a hydroxide. In these cases the oxygenation occurs through hydroxylation of the substrate. Hydrogen atom abstractions and hydroxylations can be part of a reaction chain that allows to convert an unactivated substrate into another substance of higher value. A very nice example is given in **chapter 3** where it is shown how the industrially important chemical adipic acid can be obtained by oxidation of cyclohexane, using an iron-porphyrin complex.

One goal of this research was to gain a better understanding for the reactivity of the iron-oxo group. More precisely, the question is directed towards the selectivity observed for certain iron containing metalloenzymes. Enzymes are very complex entities where many factors can be involved in the outcome of a reaction. The problem can be simplified by looking at defined biomimetic iron complexes that exhibit the same selectivity. One example is given in **chapter 4**, where it is explained why a biomimetic complex cleaves the *intradiol* bond of catechol (as opposed to *extradiol*) and what implications this has on synthetic chemistry.

The very first reaction I investigated during my PhD studies was the oxidative chlorination of unactivated substrates, a novelty for the non-heme iron chemistry. It seemed to be a promising reaction to start with, but despite looking manageable it turned out to be the most challenging part of my thesis. Even though the problem could be solved for a biomimetic complex, there was no way to explain the observed specificity of some enzymes. Gladly, newer experiments provided additional information and it was finally possible to draw a sound mechanism, which will be presented in **chapter 5**.

The last project of this thesis deals with an iron dimer, more specifically with the diamond core, a typical coordination motif found in binuclear enzymes. Most of these enzymes are very reactive and easily catalyze reactions with almost inert substrates. The diamond core is thus of great interest to synthetic chemistry. In **chapter 6** it is shown how the presence of water affects the reactivity of such a diamond core. By modeling the reaction it was possible to provide insights into the structure–reactivity relationship.

During the years of my research I realized that the most important tool of a scientist is cooperation. The presented work would be quite different without the contributions from my colleagues and friends. The adipic acid project (**Paper I**) was a combined effort of Johannes, Valentin and me, each of us looking at different steps along the reaction. Together with Valentin it was also possible to solve the mystery of the intradiol cleavage (**Paper II**). The research on the oxidative chlorination catalyzed by enzymes was initiated by Tomasz who also provided fresh ideas that finally lead to an explanation of

the enzymatic specificity (**Paper III**). Finally, it would have been impossible to investigate the reactivity of the iron dimer without dividing the quite extensive work between Johannes and me (**Paper V**).

This thesis now marks the end of my 54 months lasting PhD studies. Looking back I can say that this was the most fulfilling and contented time of my life so far (apart from childhood). During this time I found support from many people that I would like to thank at this point. First of all I thank my two supervisors Margareta and Per for inviting me to Stockholm and letting me join their research group. I am also thankful for all the advices, explanations and the guidance whenever I was in the need of help. I also thank my colleagues and friends that made my stay here such a pleasant time: Maria, Kata, Chen, Sandra, Tomek, Sven, Sten, Johannes, Valyo, Polina, Mattias, Pernilla, Saturo, Mike, Kjartan and Ola. Furthermore, I particularly want to thank Sven for providing his useful program (xyz-viewer), as well as Sandra, Johannes and Valyo for the discussions and for proof-reading this thesis.

Schließlich möchte ich meinen Eltern Karin und Erhard Noack sowie meiner Großmutter Elli Ulbrich danken, die mich während des gesamten Studiums und der Doktorarbeit mit allen Kräften unterstützt haben. Ausserdem danke ich meiner Freundin Sonja für ihre Nachsichtigkeit und die hilfreichen Kommentare.

Holger Noack
Stockholm
April 2010

List of Papers

The present dissertation is based on the papers listed below. I was involved in the calculations and in the writing of all the papers except for **paper III**, where my contribution is limited to calculations on the alternative substrate. The full text articles are appended at the end of this thesis and are reproduced with permission of the copyright holders.

I. Theoretical Insights into Heme Catalysed Oxidation of Cyclohexane to Adipic Acid
Holger Noack, Valentin Georgiev, Adam Johannes Johansson, Margareta R. A. Blomberg and Per E. M. Siegbahn
Chem. Eur. J. **2010**, submitted

II. A DFT Study on the Catalytic Reactivity of a Functional Model Complex for Intradiol-Cleaving Dioxygenases
Valentin Georgiev, Holger Noack, Thomasz Borowski, Margareta R. A. Blomberg and Per E. M. Siegbahn
J. Phys. Chem. B **2010**, accepted

III. Mechanism of Selective Halogenation by SyrB2 - a Computational Study
Thomasz Borowski, Holger Noack, Mariusz Radoń, Konrad Zych and Per E. M. Siegbahn
J. Am. Chem. Soc. **2010**, submitted

IV. Theoretical investigation on the oxidative chlorination performed by a biomimetic non-heme iron catalyst
Holger Noack and Per E. M. Siegbahn
J. Biol. Inorg. Chem. **2007**, 12, 1151–1162

V. Observed enhancement of the reactivity of a biomimetic diiron complex by the addition of water - mechanistic insights from theoretical modeling
Adam Johannes Johansson, Holger Noack, Per E. M. Siegbahn, Genqiang Xue, Lawrence Que Jr.
Dalton Trans. **2009**, 34, 6741–6750

Contents

1

Theoretical Background

This chapter introduces the central concepts of quantum chemistry. First the Schrödinger equation is presented and the classical way to solve it to a first approximation, using the Hartree-Fock method. Based on that density functional theory is introduced, which is the method used for all the calculations in this thesis. Finally, the connection from the microscopic to the macroscopic world is established, using statistical mechanics and thermochemistry.

1.1 The Schrödinger Equation

Since microscopic particles, such as electrons and protons, are subjected to the Heisenberg[1] uncertainty principle, it is not possible to treat them by deterministic equations, as it is the case for macroscopic particles in classical mechanics. In quantum mechanics the existence of a function Ψ is assumed. This state- or wavefunction Ψ depends on the coordinates x of a particle and contains all possible information about the system. For a one-dimensional one-particle system Erwin Schrödinger[2] presented an equation of the form

$$-\frac{\hbar^2}{2m}\frac{\partial^2\Psi(x,t)}{\partial x^2} + V(x,t)\Psi(x,t) = \frac{\hbar}{i}\frac{\partial\Psi(x,t)}{\partial t} \tag{1.1}$$

that describes how the state of the system is changing with time. Therefore, eq. 1.1 is called *time-dependent* Schrödinger equation. The first term on the

[1] Werner Heisenberg, 1901–1976, a German physicist best known for the uncertainty principle that he presented in 1926, one year after his matrix formulation of quantum mechanics, for which he received the Nobel prize in 1932.

[2] Erwin Schrödinger, 1887–1961, was an Austrian physicist. The equation he published in 1926 was a breakthrough for quantum mechanics, he was rewarded with the Nobel prize in 1933.

left hand side stands for the kinetic energy of a particle with mass m, the second term $V(x,t)$ describes the potential energy of this particle. If no time-dependent forces act upon the system the potential energy becomes time-independent, $V = V(x)$, and the time-dependence can be separated out to give the *time-independent* Schrödinger equation

$$-\frac{\hbar^2}{2m}\frac{d^2\psi(x)}{dx^2} + V(x)\psi(x) = E\psi(x)\ . \tag{1.2}$$

For the three-dimensional case the equation has to be differentiated over all space, which can be done by inserting the Laplace operator ∇^2, leading to the time-independent Schrödinger equation for the three-dimensional case.

$$-\frac{\hbar^2}{2m}\nabla^2\psi(x,y,z) + V(x,y,z)\psi(x,y,z) = E\psi(x,y,z) \tag{1.3}$$

Since the right and the left hand side of this equation must have the same dimension it follows that the constant E represents the total energy of the system. If the operators for kinetic and potential energy are summarized in the Hamilton[3] operator $\hat{H}$ the well known operator form of the Schrödinger equation is obtained.

$$\hat{H}\Psi = E\Psi \tag{1.4}$$

For a system composed of N electrons and M nuclei the Hamiltonian contains the kinetic energy T of those particles and all kinds of potential interaction V.

$$\mathbf{H} = \mathbf{T}_e + \mathbf{T}_n + \mathbf{V}_{ne} + \mathbf{V}_{ee} + \mathbf{V}_{nn} \tag{1.5}$$

In particular these terms stand for the kinetic energy of the electrons $\mathbf{T}_e$ and the nuclei $\mathbf{T}_n$, the attractive interactions between electrons and nuclei $\mathbf{V}_{ne}$, as well as repulsive interactions among electrons $\mathbf{V}_{ee}$ and nuclei $\mathbf{V}_{nn}$. Within the adiabatic Born-Oppenheimer[4] approximation the movement of electrons and nuclei can be separated, i.e. the correlation between them is eliminated. Thus, all that remains is to solve the time-independent *electronic* Schrödinger

[3] William Rowan Hamilton, 1805–1865, was an Irish physicist, mathematician and astronomer, who reformulated the Newtonian mechanics. The so-called Hamiltonian mechanics were used to derive the Hamilton-Jacobi equation, the closest approach of classical mechanics to quantum mechanics.

[4] Max Born, 1882–1970, was a German physicist and mathematician who won the Noble prize in 1954 for his statistical interpretation of the wavefunction. J. Robert Oppenheimer, 1904–1967, was an American physicist, unfortunately best known for his role in developing the first nuclear weapon.

equation for a given set of nuclear coordinates ($\mathbf{T}_n = 0$ and $\mathbf{V}_{nn} = const.$) to obtain the energy of the system.

1.2 The Hartree-Fock Method

Within the Hartree-Fock[5] method the Hamilton operator is formulated as a sum of one- and two-electron operators.

$$\mathbf{H}_{el} = \sum_{i}^{N} \mathbf{h}_i + \sum_{i}^{N} \sum_{j \geq i}^{N} \frac{1}{r_{ij}} \qquad \text{where} \qquad \mathbf{h}_i = -\frac{1}{2}\nabla_i^2 - \sum_{A}^{M} \frac{Z_A}{r_{iA}} \tag{1.6}$$

Here, the movement of electrons in the field of the nuclei is summarized in the sum of one-electron operators $\mathbf{h}_i$. The two-electron term r_{ij}^{-1} describes the electrostatic potential $\mathbf{V}_{ee}$ and depends on all pairwise interactions between the electrons. Due to this *inter*-electronic correlation it is impossible to solve the Schrödinger equation exactly, except for one electron systems like the hydrogen atom or the helium cation (2-body systems).

However, it is possible to approximate the solution by reformulating the problem of the unknown many-electron wavefunction as one that is composed out of many one-electron functions. Since electrons are fermions this one-electron wavefunction has to be antisymmetric with respect to the interchange of two electron coordinates. For a system containing N electrons this condition is fulfilled by the so-called Slater[6] determinant.

$$\Psi_{SD}(1,2,\dots N) = \frac{1}{\sqrt{N!}} \begin{vmatrix} \phi_1(1) & \phi_2(1) & \cdots & \phi_N(1) \\ \phi_1(2) & \phi_2(2) & \cdots & \phi_N(2) \\ \vdots & \vdots & \ddots & \vdots \\ \phi_1(N) & \phi_2(N) & \cdots & \phi_N(N) \end{vmatrix} \tag{1.7}$$

Herein, the spin-orbitals ϕ_i are composed out of a space function $\psi(x)$ and a spin function α or β. Using this wavefunction the electronic energy can be calculated following the variation principle, which states that the energy obtained from calculations with an approximate wavefunction is always an upper bound to the exact ground-state energy. The system is thus best described by a wavefunction that gives the lowest possible energy.

[5]Douglas Hartree, 1897–1958, was an English physicist and mathematician most famous for his development of numerical analysis. The atomic unit of energy is named after him. Vladimir Aleksandrovich Fock, 1898–1974, was a Russian physicist contributing outstanding work in many different fields. He wrote the first text book on quantum mechanics in 1931.

[6]John Clarke Slater, 1900–1976, was an American physicist and chemist. His idea to express antisymmetric wavefunctions in the form of determinants was developed in 1929. Furthermore, he introduced exponential functions to describe atomic orbitals in 1930.

To this purpose the single determinant wavefunction has to be optimized, which can only be done by variation of its spin orbitals. This is done using an effective one-electron operator, the Fock operator $\mathbf{F}_i$, which is accounting for the electron-electron interaction via a *mean* potential $\mathbf{v}_i^{HF}$.

$$\begin{aligned}\mathbf{F}_i =& \mathbf{h}_i + \mathbf{v}_i^{HF} \\ =& \mathbf{h}_i + \sum_j \left(\mathbf{J}_j - \mathbf{K}_j\right)\end{aligned} \tag{1.8}$$

The Hartree-Fock potential is composed out of a Coulomb[7] term **J** and an exchange term **K**. Both terms result by the action of the two-electron operator $\mathbf{r}_{ij}^{-1}$ from equation 1.6 on two spin functions of the determinant. The operation of the Coulomb term **J** on electron 1 in spin-orbital ϕ_i is defined as

$$\mathbf{J}_j(1)\phi_i(1) = \left[\int \phi_j^*(2)\frac{1}{r_{12}}\phi_j(2)d\tau_2\right]\phi_i(1)\ . \tag{1.9}$$

The exchange term **K** is a direct consequence of the antisymmetry of the determinant and causes an exchange of electron 1 and electron 2.

$$\mathbf{K}_j(1)\phi_i(1) = \left[\int \phi_j^*(2)\frac{1}{r_{12}}\phi_i(2)d\tau_2\right]\phi_j(1) \tag{1.10}$$

Within the Hartree-Fock approximation electron 1 in orbital ϕ_i experiences an *one-electron potential* by electron 2. Through summation over all j in equation 1.8 one arrives at the mean potential exerted by all $N-1$ electrons in the other spin-orbitals on electron 1 in spin-orbital ϕ_i. Self interaction with the own orbital ($j = i$) is canceled out.

$$\left[\mathbf{J}_i(1) - \mathbf{K}_i(1)\right]\phi_i(1) = 0 \tag{1.11}$$

The Hartree-Fock equation is a pseudo-eigenvalue equation and has to be solved iteratively, since the operation of **J** and **K** has a functional dependence on the shape of all spin orbitals. To begin with, the unknown orbitals are approximated by a linear combination of known basis functions χ_α.

$$\mathbf{F}_i \sum_\alpha^M c_{\alpha i}\chi_\alpha = \varepsilon_i \sum_\alpha^M c_{\alpha i}\chi_\alpha \tag{1.12}$$

Since the basis functions are known, only their coefficients have to be

[7] Charles-Augustin de Coulomb, 1736–1806, was a French physicist who in 1783 published a law to describe the electrostatic interaction between charged particles.

determined. Multiplication with a specific basis function and integration gives the Roothaan-Hall[8] equations [1,2]. All M equations are collected in an equation of matrices

$$\mathbf{FC} = \mathbf{SC}\boldsymbol{\varepsilon} \tag{1.13}$$

wherein $\mathbf{F}$ is the matrix of the Fock operator, $\mathbf{S}$ is the overlap matrix, $\mathbf{C}$ the coefficient matrix, and $\boldsymbol{\varepsilon}$ the diagonal energy matrix. The optimization procedure begins by guessing a set of coefficients. Then the Fock matrix is formed and diagonalized. From the resulting set of coefficients a new matrix is constructed and the process repeats itself until the field generated by the electrons reaches consistency. The final energy expression resulting from the Hartree-Fock method is thus

$$E = \sum_{i=1}^{N} h_i + \frac{1}{2}\sum_{i}^{N}\sum_{j>i}^{N}(J_{ij} - K_{ij}) + V_{nn} \tag{1.14}$$

wherein the factor $1/2$ corrects the double counting of the electron-electron interaction.

Within the one electron approximation made in Hartree-Fock theory the electronic interaction is described by a mean potential. In the real world, however, the movement of the electrons is correlated. The difference between the Hartree-Fock energy and the real ground-state energy is thus the correlation energy. For a pair of valence electrons of opposite spin this correlation energy has the magnitude of $1eV$ which is in the energetic range of chemical reactions [3].

1.3 Density Functional Theory

The method described previously was based on the concept of wavefunctions and provided a solution to the electronic Schrödinger equation. In contrast, density functional theory is based on the electron density $\rho(r)$, an observable that can be measured experimentally. Furthermore, for a N electron system it depends only on 3 coordinates, whereas a wavefunction would depend on $3N$ coordinates. Two theorems formulated by Hohenberg and Kohn[9] build the foundation of density functional theory [4]. The first theorem is

[8]Clemens C. J. Roothaan, born 1918 in the Netherlands, developed a representation for the Hartree-Fock equation in 1951. George Garfield Hall, born 1925 in Ireland, came independently to the same result for which he was awarded with a PhD degree.

[9]Pierre C. Hohenberg is an American physicist with main interest in condensed matter physics. Walter Kohn, born 1923 in Austria, laid the foundations of density functional theory together with Hohenberg in 1963 during a sabbatical semester in Paris. He was the driving force

the existence theorem which states that the external potential $v_{ext}(r)$ has a functional dependency on the electron density. With knowledge of this potential it is possible to construct a Hamilton operator which in turn can be used to derive a wavefunction. That way it is possible to calculate the ground-state energy. The latter has thus a functional dependency on the electron density.

$$\rho_0(r) \Rightarrow v_{ext}(r) \Rightarrow \mathbf{H} \Rightarrow \Psi_0 \Rightarrow E_0 \quad \text{which means} \quad E_0 = F\left[\rho_0(r)\right]$$

The second theorem is the variational theorem stating that the exact functional $F\left[\rho(r)\right]$ only then returns the lowest possible energy, if the density used in the calculations is the true ground-state electron density. In other words, the electron density is subjected to the variational principle.

However, it is neither known how the electron density can be found without setting up a wavefunction first, nor how the exact energy functional is composed in detail. In analogy to equation 1.5 such functional can be parted in kinetic and potential energy terms.

$$F\left[\rho\right] = T\left[\rho\right] + V_{ne}\left[\rho\right] + V_{ee}\left[\rho\right] \tag{1.15}$$

The nuclei-electron interaction $V_{ne}\left[\rho\right]$ can be described classically using the charge distribution $\rho(r)$. The electron-electron interaction $V_{ee}\left[\rho\right]$ can be approximated by the Coulomb term $J\left[\rho\right]$, where the factor of $1/2$ corrects for the double counting of the charge clouds $\rho(r)$ and $\rho(r')$.

$$\begin{aligned} V_{ne}\left[\rho\right] &= -\sum_A \int \frac{Z_A \rho(r)}{|r - R_A|} dr \\ V_{ee}\left[\rho\right] &\simeq J\left[\rho\right] = \frac{1}{2} \int \int \frac{\rho(r)\rho(r')}{|r - r'|} dr dr' \end{aligned} \tag{1.16}$$

To be able to describe the kinetic energy $T\left[\rho\right]$ one needs to act on the assumption of a reference system of non-interacting electrons. The electrons of this reference system all experience the same external potential $v_{ref}(r)$, which is chosen in a way that its corresponding ground-state density $\rho_{ref}(r)$ equals the exact ground-state density $\rho_0(r)$ for the system of interacting electrons. This renders it possible to use the Slater determinant to set up a wavefunction for the non-interacting system and the kinetic energy can be found in analogy to the Hartree-Fock method.

$$T_{ref}\left[\rho\right] = -\frac{1}{2} \sum_i \langle \phi_i | \nabla_i^2 | \phi_i \rangle \tag{1.17}$$

behind the further development of modern density functional theory, for which he received the Nobel prize 1998.

The difference between the reference system and the real system is summarized in the exchange-correlation functional $E_{XC}[\rho]$. This concerns the uncorrelated movement of the electrons $T_{ref}[\rho]$ as well as the approximation of the exact electronic interaction by the Coulomb term $J[\rho]$.

$$\begin{aligned} \Delta T[\rho] &= T[\rho] - T_{ref}[\rho] \\ \Delta V_{ee}[\rho] &= V_{ee}[\rho] - J[\rho] \\ E_{XC}[\rho] &= \Delta T[\rho] + \Delta V_{ee}[\rho] \end{aligned} \tag{1.18}$$

Since the ground state of the reference system can be described by a Slater determinant the complete energy functional takes the form

$$\begin{aligned} F[\rho(r)] = & -\frac{1}{2}\sum_i \langle\phi_i|\nabla_i^2|\phi_i\rangle - \sum_i\sum_A \langle\phi_i|\frac{Z_A}{|r-R_A|}|\phi_i\rangle \\ & + \sum_i \langle\phi_i|\frac{1}{2}\int\frac{\rho(r')}{|r-r'|}dr'|\phi_i\rangle + E_{XC}[\rho] \end{aligned} \tag{1.19}$$

and magically one is back using single-electron wavefunctions to solve the density dependent energy functional. If the exact expression for the exchange-correlation functional $E_{XC}[\rho]$ would be known the true ground-state energy of the system could be obtained. However, fact is that the exchange-correlation functional $E_{XC}[\rho]$ has to be approximated, and several approximations have been suggested. It would go beyond the scope of this thesis to go into details regarding the development of modern density functionals, therefore only three of the historically most important types of functionals will be presented in the following.

Local Spin Density Approximation

The local spin density approximation (LSDA) of the exchange-correlation functional is based on the assumption of a homogeneous electron-gas, for which the local density $\rho(r)$ is constant at each point in space r. $E_{XC}[\rho]$ is separated into an exchange functional $E_X[\rho]$ and a correlation functional $E_C[\rho]$. The functional for the exchange energy of a homogeneous electron-gas has the form

$$\varepsilon_X^{LSDA}[\rho_\alpha,\rho_\beta] = -\frac{3}{4}\left(\frac{6}{\pi}\right)^{1/3}\int\left(\rho_\alpha^{1/3}(r)+\rho_\beta^{1/3}(r)\right)dr\,. \tag{1.20}$$

No analytical functional can be given for the correlation energy $E_C[\rho]$. However, by calculating the energy of an uniform electron gas for different densities, the correlation energy can be estimated by subtraction of the analytic exchange energy [5]. Through analytical interpolation of these

results it was possible to formulate a functional for the correlation energy $E_C^{VWN}[\rho]$ [6].

Generalized Gradient Approximation
Within the generalized gradient approximation (GGA), the electron density is not anymore considered to be homogeneous by taking the gradient g of the density into account. One popular GGA exchange functional was formulated by Becke[10] in 1988 [7].

$$\begin{aligned} \varepsilon_X^{B88} =& \varepsilon_X^{LSDA} + \Delta\varepsilon_X^{B88} \\ \Delta\varepsilon_X^{B88} =& -\beta\rho^{1/3}\frac{g^2}{1+6\beta g sinh^{-1}g} \end{aligned} \tag{1.21}$$

Herein β is a parameter that was fitted to the experimental data of inert gases. For the correlation energy $E_C[\rho]$ there are two popular functionals to mention. The *P86*-functional [8] is based on the LSDA correlation and contains an additional fit to match the correlation energy of the neon atom. *LYP* on the other hand is derived from an expression describing the correlation energy of the helium atom [9]. It contains four parameters that were fitted to experimental data of helium.

Hybrid functionals
In absolute numbers, contributions from the exchange energy are significantly larger than those originating from the electron correlation [10]. A better description of the electronic exchange part could thus improve the result. One way for enhancement is given by using the known exchange term of an uncorrelated system, as it is done in Hartree-Fock theory. The correlated and the uncorrelated states of the system are then coupled via the adiabatic connection formalism [11].

$$E_{XC}^{ACF} = E_X^{HF} + \lambda\left(E_{XC}^{DFT} - E_X^{HF}\right) . \tag{1.22}$$

If the coupling parameter λ is between zero and one exchange-correlation energy of a correlated system E_{XC}^{DFT} is taken into account (via the LSDA or GGA formalism). The functional used in this thesis, *B3LYP*, was constructed by Becke and captures 20 percent of the exchange energy using Hartree-Fock exchange E_X^{HF} [12].

$$E_{XC}^{B3LYP} = aE_X^{HF} + (1-a)\,E_X^{LSDA} + b\Delta E_X^{B88} + c\Delta E_C^{LYP} + (1-c)\,E_C^{VWN} \tag{1.23}$$

The three coefficients a, b and c were obtained by a fit to experimental data

[10] Axel D. Becke, born 1953 in Germany, contributed to the widespread use of density functional theory through the development of high quality exchange-correlation functionals.

from the ten elements out of the first two periods (56 atomization energies, 42 ionization potentials, 8 proton affinities and total energies).

With the complete energy functional at hand the electronic energy can be calculated by variation of the electron density. This is done by varying the molecular orbitals ϕ_i of the non-interacting reference system using the self consistent field approach.

Limitations

Self Interaction

Self interaction describes the unphysical phenomenon of an electron interacting with its own density. This artifact is due to the approximate description of the exchange term within the density functional. In Hartree-Fock theory Coulomb and exchange term were both described exactly, and thus cancelled to zero in case of self interaction (see equations 1.9 to 1.11). This, however, is not the case in density functional theory where the difference between these two terms is not zero. For the majority of chemical systems self interaction causes no problem. However, in some cases *delocalization* of the electron density is favored to lower the electronic self-repulsion, which possibly becomes important for bond dissociation, charge transfer complexes [13] and charged radical systems [14, 15].

It should be noted that this electronic self repulsion is partly cancelled by the Hartree-Fock exchange introduced in hybrid functionals. Other functionals have been constructed to completely remove self interaction by enforcing Coulomb and exchange term to cancel each other for an unpaired electron. Interestingly, such functionals perform much worse in benchmark tests than ordinary functionals [16], which led to the suggestion that self interaction contributes to the high accuracy of density functionals by mimicking long range (non-dynamic) correlation effects [17].

Dispersion

Dispersive interactions are long-range electron correlations describing the attractive part in van der Waals[11] forces [18, 19]. In general, dispersive interactions result from mutually induced dipoles between molecules (electrostatic interactions) and they play important roles for large molecules like DNA and proteins. As described previously, such correlation effects are only approximated in density functionals, which leads to the neglect of dispersion energy and thus to an overestimation of the repulsion between bulky groups.

[11] Johannes Diderik van der Waals, 1887–1923, was a Dutch physicist, best known for his popular equation of state that he derived in his doctoral thesis on the continuity of the gas and the liquid state in 1873. Moreover, he was one of the first to postulate an intermolecular force that is now named after him.

A pragmatic way to incorporate dispersion is to add an empirical potential of the form $C_6 R^{-6}$ on top of the calculated energy [20,21].

$$E_{disp} = -s_6 \sum_{ij} \frac{C_{6,ij}}{R_{ij}^6} f_{dmp}(R_{ij}) \tag{1.24}$$

The global scaling factor s_6 depends on the density functional used to calculate the dispersion free energy, $C_{6,ij}$ denotes the dispersion coefficient for atom pair ij, and R_{ij} is the interatomic distance. A damping function f_{dmp} must be used to avoid near-singularities for small distances R,

$$f_{dmp}(R_{ij}) = \frac{1}{1 + e^{-d(R/R_0 - 1)}} \tag{1.25}$$

wherein R_0 denotes the sum of atomic van der Waals radii and d the steepness of the function. The damping function f_{dmp} decays for small R fast enough to zero such that the dispersion corrections between atoms below their typical van der Waals distance are negligible. This is to make sure that "normal" bonds are not significantly affected by the correction.

Broken Symmetry

Very common for transition metal containing systems is that they are many unpaired electrons which can be coupled in different ways. High-spin states result from ferromagnetic coupling and are pure spin states within the single-determinant approach of density functional theory. The problem arises for low-spin states resulting from antiferromagnetic coupling of the unpaired electrons. In this case the eigenstates of the energy operator are no longer eigenfunctions of the total spin operator $\langle \hat{S}^2 \rangle$, in other words, low-spin states resulting from antiferromagnetic coupling are spin contaminated by their corresponding high spin states, which affects the calculated energy associated to them.

The energy of such a broken symmetry state can be corrected by applying the Heisenberg Hamiltonian formalism for weak spin coupling together with Landés[12] interval rule [22, 23]. For the two electron case the correction is simple and an example is given below. The Heisenberg Hamiltonian has the form

$$H_{spin} = J S_A S_B \tag{1.26}$$

wherein J is the exchange coupling parameter and S_A and S_B are the spins

[12] Alfred Landé, 1888-1976, was a German physicist who studied under supervision of Arnold Sommerfeld in Munich. His main contribution is the introduction of the Landé g-factor for electrons.

on atom A and B. The energies of the high-spin E_{HS} and the low-spin state E_{LS} are thus

$$\begin{aligned} E_{HS} &= JS_AS_B \\ E_{BS} &= JS_A(-S_B) = -JS_AS_B \end{aligned} \tag{1.27}$$

The exchange coupling parameter J can thus be obtained from the energetic difference between high spin and low spin state.

$$J = \frac{E_{HS} - E_{BS}}{2S_AS_B} \tag{1.28}$$

Now that the coupling parameter is known the correction to the broken symmetry spin state can be calculated by applying Landés interval rule. In this particular case of singlet-triplet splitting the true low spin energy is

$$E_{LS} = E_{HS} - J \tag{1.29}$$

The correction will always increase the spin splitting between low-spin and high-spin state. If the energy of the broken symmetry state is below that of the high-spin state, the correction will further lower the low-spin state, and in the opposite case of an energetic lower lying high-spin state the correction will raise the low-spin state.

Accuracy

Since the development of hybrid functionals led to a widespread use of density functional theory a number of benchmark tests has been provided to test the accuracy of the various functionals. The most extensive test so far is on the G3/05 dataset [24], consisting of 454 accurate experimental thermochemical values, that were measured with a quoted uncertainty of less than 1 kcal/mol. For this test B3LYP shows a mean absolute deviation of 4.11 kcal/mol, see table 1.1.

If the system contains transition metals the accuracy of B3LYP is more difficult to evaluate since less experimental data is available. For first row transition metal compounds of the form MR^+, where R = H, CH_2, CH_3, or OH, the mean absolute deviation for bond dissociation is in the range 3.6-5.5 kcal/mol [25,26]. B3LYP has also been tested on the bond dissociation energies of metal carbonyl complexes for Cr, Mo, W, Fe and Ni, revealing a mean absolute deviation of 2.6 kcal/mol [25, 27]. It has therefore been estimated that an average error of 3-5 kcal/mol can be expected when applying B3LYP on calculations of transition metal complexes [28].

	B3LYP
Enthalpies of formation (270)	4.63
Ionization energies (105)	3.83
Electron affinities (63)	2.99
Proton affinities (10)	1.39
Hydrogen-bonded complexes (6)	1.19
Total (454)	4.11

Table 1.1: *Mean absolute deviations (kcal/mol) for the B3LYP functional on the G3/05 dataset [24].*

1.4 Thermochemistry

The energy obtained from quantum chemical calculations within the Born-Oppenheimer approximation is the pure electronic energy ϵ_{elec} of a molecular system. To calculate the values of macroscopic properties such as enthalpy, entropy or Gibbs[13] free energy one needs to make use of statistical thermodynamics. The central concept is the partition function q, which is the probability weighted sum of energy states

$$q = \sum_{i}^{\infty} e^{-\epsilon_i / k_B T} \tag{1.30}$$

wherein k_B is the Boltzmann[14] constant. The partition function can be parted into electronic, translational, rotational and vibrational contributions. The electronic energy is taken directly from the quantum chemical calculation, since only the ground state is occupied at room temperature[15]. The translational and rotational partition functions are trivially calculated from the mass of the particle and the temperature. The most difficult part is the vibrational contribution, which is calculated from all the vibrational normal modes of a molecule, by using the harmonic approximation.

[13]Josiah Willard Gibbs, 1839–1903, was an American physicist, chemist and mathematician. He built the theoretical framework of thermochemistry and influenced many great scientist of the 20th century. Unfortunately, he received only few recognition during his lifetime, partly because his work was published in English at a time when german was the leading language in chemistry.

[14]Ludwig Eduard Boltzmann, 1844–1906, was an Austrian physicist with major contributions to statistical mechanics. The Boltzmann constant forms a bridge between the microscopic and the macroscopic world by relating the energy of a microscopic particle to the temperature. It is the gas constant R divided by the Avogadro number N_A ($k_B = 1.3807 \cdot 10^{-23}$ J/K).

[15]The term "room temperature" refers to a temperature of 20°C. A quite optimistic assessment compared to the temperature of some student apartments during the winter.

$$U(\Delta R) = \frac{1}{2}\frac{d^2E}{dR^2}\Delta R^2 = \frac{1}{2}k\Delta R^2 \tag{1.31}$$

The force constant k in eq. 1.31 is obtained by forming the second derivative of the energy with respect to the internal coordinates. With knowledge of the force constants k and the reduced mass μ of the vibrating parts the vibrational modes can be calculated.

$$\nu = \frac{1}{2\pi}\sqrt{\frac{k}{\mu}} \tag{1.32}$$

The energy connected to the vibration of a nonlinear molecule consisting of N atoms is then given by

$$\epsilon_{vib} = \sum_{i}^{3N-6}(n_i + \frac{1}{2})h\nu_i \,. \tag{1.33}$$

If all energetic contributions to the one-particle partition function are known, the corresponding partition function for a system of N non-interacting identical particles is easily obtained

$$Q = \frac{1}{N!}q^N \tag{1.34}$$

and can be used to derive thermodynamic properties like enthalpy H, entropy S and Gibbs free energy G.

$$\begin{aligned} H =& k_b T^2 \left(\frac{\delta ln Q}{\delta T}\right)_V + k_b T \left(\frac{\delta ln Q}{\delta V}\right)_T \\ S =& k_b T \left(\frac{\delta ln Q}{\delta T}\right)_V + k_b ln Q \\ G =& H - TS = k_b T \left(\frac{\delta ln Q}{\delta V}\right)_T - k_b T ln Q \end{aligned} \tag{1.35}$$

1.5 Transition State Theory

Transition state theory (TST) uses the concept of potential energy surfaces, where it connects two minima via a minimum energy pathway, also called reaction coordinate. The highest point along this reaction coordinate is the transition state (activated complex). Figure 1.1 shows the energy profile for a chemical reaction in which molecule AX transfers atom X to molecule B, passing through an activated complex $[AXB]^{\ddagger}$.

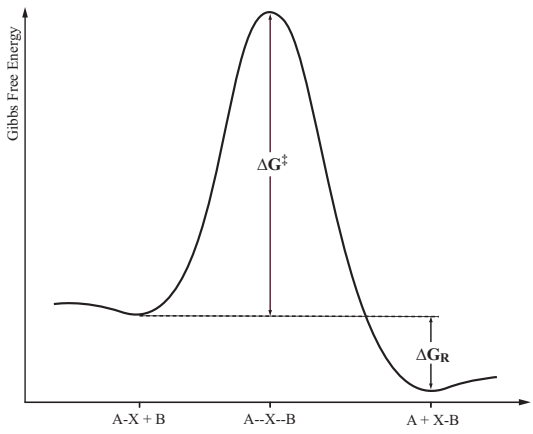

Figure 1.1: *Potential energy surface showing the minimum energy path of a one step chemical reaction.* $\Delta G^{\ddagger}$ *defines the activation barrier and* ΔG_R *reaction energy.*

$$AX + B \rightleftharpoons [AXB]^{\ddagger} \rightarrow A + BX$$

The reaction is characterized by an activation barrier $\Delta G^{\ddagger}$ determining the kinetics of the reaction, and a reaction energy ΔG_R determining the thermodynamics. Kinetic data is experimentally accessible via the rate of a reaction, and that is where transition state theory builds the bridge to the calculated energetics, as shown in the following. The chemical equilibrium between the activated complex and the reactants is characterized by the equilibrium constant $K^{\ddagger}$.

$$K^{\ddagger} = \frac{[AXB]^{\ddagger}}{[AX][B]} \tag{1.36}$$

Within Boltzmann statistics the equilibrium constant $K^{\ddagger}$ can be expressed by the difference in Gibbs free energy $\Delta G^{\ddagger}$ between reactants and transition state.

$$K^{\ddagger} = e^{-\Delta G^{\ddagger}/RT} \tag{1.37}$$

According to TST the rate of the reaction is proportional to the concentration of the activated complex $[AXB]^{\ddagger}$. This complex is very short lived and decays to the products during the first vibrational excursion ν. Using Planck's law this vibration has the form

$$\nu = \frac{k_B T}{h} \, . \tag{1.38}$$

It follows the Eyring[16] equation that combines the experimentally observable rate constant k with the Gibbs free energy of the activation barrier.

$$k = \kappa \frac{k_B T}{h} e^{\Delta G^{\ddagger}/RT} \tag{1.39}$$

The transmission coefficient κ accounts for tunneling of the reaction barrier as well as recrossing to the reactant side. For most reactions this coefficient can be set to unity. A phenomenon typically observed for first row transition metal complexes is the crossing of two potential energy surfaces corresponding to different spin states during the course of a reaction [29]. In this case the rate is affected by the magnitude of the spin orbit coupling, which enters the Eyring equation as being part of a probability factor for the spin transition. However, even in cases of relatively weak spin orbit coupling the rate is not expected to decrease by more than a factor of 10-100 [30], which corresponds to an increase in activation energy of 1.4 to 2.8 kcal/mol and is thus within the accuracy of the B3LYP functional.

From figure 1.2 it can be seen that a rate of $1s^{-1}$ corresponds to an activation barrier of 17.1 kcal/mol at room temperature. An enzyme catalyzing a reaction at ambient conditions with a rate faster than 10^4 s^{-1} must have an activation barrier below 12.0 kcal/mol.

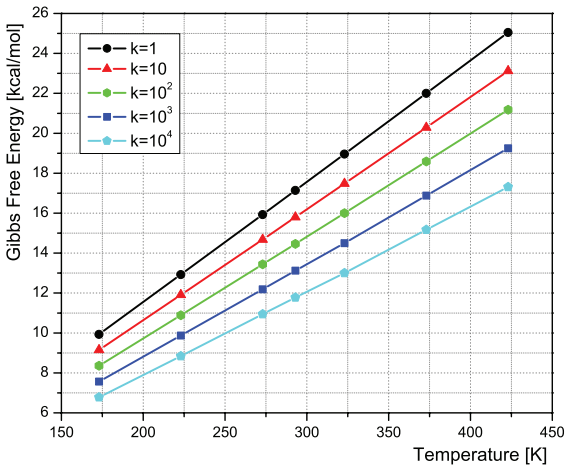

Figure 1.2: *Temperature dependence of the activation energy for different rates.*

[16]Henry Eyring, 1901–1981, was an American chemist who studied reaction rates and intermediates. The Eyring equation was simultaneously developed by Eyring, M. G. Evans and M. Polanyi in 1935, but none of them was awarded with a Nobel prize.

2

Biochemistry of Iron

Iron, symbolized by Fe[1], is one of the most abundant elements in the lithosphere, it comes fourth after oxygen, silicium and aluminum [31]. However, looking at the elements distribution in the ocean one can see iron far behind. This is due to irons existence as Fe(III) under the oxidative atmosphere present on earth, leading to the formation of insoluble oxides like Magnetite, Fe_3O_4, or Hematite, Fe_2O_3. Hydroxide complexes formed by iron at this oxidation state are hardly soluble at pH 7. For example, the solubility product of $Fe(OH)_3$ (also known as red mud, a side product of aluminium production from Bauxite) is only 10^{-38} M^4 [32]. And yet, iron is taking part in the chemistry of life and is the most abundant transition metal in the human body [31]. So obviously, there must be mechanisms making iron available for the processes of life.

2.1 Bioavailability

Bioavailability of iron is provided by a group of chelating agents. Yeast, bacteria and fungi use so-called siderophores which have a high affinity for Fe(III) and form very stable complexes. Higher organisms use L-ascorbate (vitamin c) to chelate iron. These substances have in common that they are of low molecular weight, soluble and able to penetrate membranes. Regarding their coordination siderophores are divided in two major classes, hydroxamates and catecholates, see Figure 2.1. Both, the siderophores and L-ascorbate, form unsaturated five-membered ring systems free of tension, with anionic oxygen coordination. In accordance to HSAB theory [33], the

[1] In ancient times iron used to be represented by the symbol for Mars ♂. A proper choice given that a) there is a high concentration of ferric iron on the (reddish) surface of Mars, and b) ancient weapons were made from iron and Mars was the god of war.

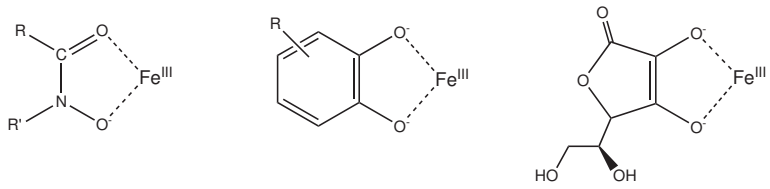

Hydroxamate coordiantion Catecholate coordination L-ascorbate coordination

Figure 2.1: *Comparison of Fe(III) coordination by two different types of siderophores and L-ascorbate.*

concept of hard and soft acids and bases, the hard Lewis[2] acid Fe(III) forms stable complexes with hard bases like O^{2-}, OH^-, RO^-, Cl^-, NH_3 and ClO_4^-. Corresponding complexes with Fe(II) are less stable due to irons lower charge and a larger ion radius. Thus, iron would be released from the siderophores by reduction and made available for processes in biochemistry. If not used immediately free Fe(II) would be problematic for any organism, since its uncontrolled reaction with O_2 or peroxide would lead to the formation of radicals. To keep iron bioavailable it has to be stored, which is done by a large protein called ferritin consisting of an inorganic core with up to 4500 iron atoms. Here iron is stored in a structure similar to the mineral ferrihydrite, 5 Fe_2O_3 x 9 H_2O, and can therefrom be mobilized by delivery of reducing and chelating agents [34].

2.2 Heme Coordination

Generally, iron containing proteins are divided in two major classes based on the coordination motif on the iron center, heme and nonheme. The functions covered by hemoproteins are manifold. Uptake, transport and storage of O_2 is done by two proteins, hemoglobin and myoglobin. Within oxidative phosphorylation[3] heme containing cytochromes take part in electron transferring processes. And finally, the controlled conversion of oxygen containing intermediates is catalyzed by peroxidases and catalases. In hemoproteins the iron atom is coordinated by the tetrapyrrole porphyrin, a ligand that provides four nitrogen donors connected in a conjugated ring system. The axial position on the proximal site is occupied by histidine or cysteine, and the sixth coordination site is available for the substrate. As

[2]Gilbert N. Lewis, 1875–1946, was an American physicist who introduced the concept of covalent bonds in 1916.

[3]Oxidative phosphorylation describes the generation of adenosine-5′-triphosphate (ATP, a molecular unit to store energy) in the respiratory chain under consumption of O_2.

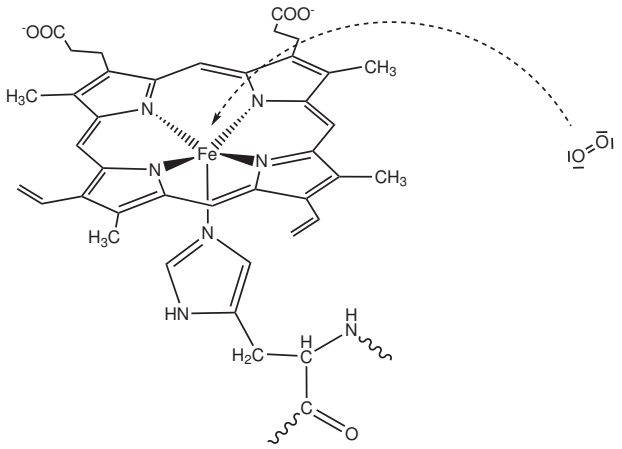

Figure 2.2: *Heme group of hemoglobin: Fe(II) is coordinated by porphyrin and histidine in axial position. The sixth coordination site is available for substrates, in this case O_2.*

an example the heme group of hemoglobin is shown in Figure 2.2. In its resting state iron exists as Fe(II), however, the conjugated porphyrin ligand is able to stabilize highly oxidized intermediates up to Fe(IV). In addition the ligand is able to temporarily provide one electron itself. One characteristic of the sixfold coordination with mainly nitrogen donors is that the energetic difference between low-spin and high-spin states is quite small, facilitating the possibility for a spin crossover at room temperature [35,36]. Although the porphyrin ligand can have different substituents, the only site available for significant ligand tuning is in axial position trans to the oxo ligand because of the planar nature of the tetradentate porphyrin cofactor.

2.3 Nonheme Coordination

Nonheme iron proteins can further be divided into two major groups. One of them consists of iron-sulfur proteins, that take part in one-electron transfer processes over large distances. Their characteristic criterion is that the iron atom is coordinated by cystein-sulfur and inorganic sulfide (S^{2-}). Depending on the degree of aggregation, four types of Fe/S units are known, see Figure 2.3. In these clusters the iron ion has a slightly distorted tetrahedric coordination due to the space required by the large sulfur ions, as compared to oxygen or nitrogen donors, which usually form a sixfold coordination. In consequence, iron possesses a high-spin configuration throughout all Fe/S clusters (decreased ligand field splitting). A common feature among

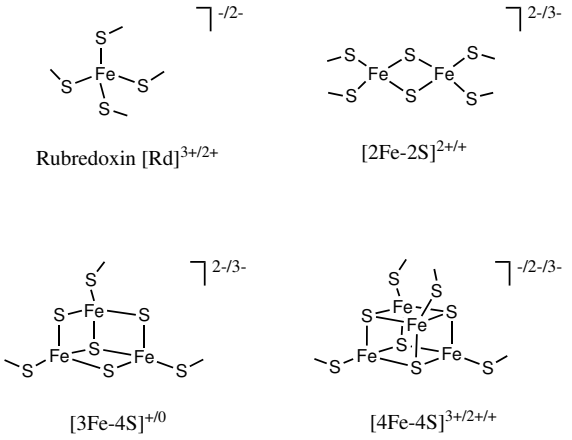

Figure 2.3: *The four general types of Fe/S centers found in iron-sulfur proteins. It can be seen that they exhibit flexibility in the choice of total charge and oxidation states.*

hemoproteins and iron-sulfur proteins is the function of their ligands as potential electron buffers, meaning that those ligands are able to provide electrons for redox processes and to stabilize the oxidation state of the iron center.

This is not the case for the other large group of nonheme iron enzymes where the iron center is mainly coordinated by amino acid residues, water and oxo-anions. Commonly used amino acids are histidine, cysteine, tyrosine, aspartate and glutamate. The remaining coordination sites are mostly occupied by water. Despite the diversity of this nonheme coordination there is one frequently found motif in which the iron ion is coordinated by two histidines and one carboxylate (glutamate or aspartate), forming a

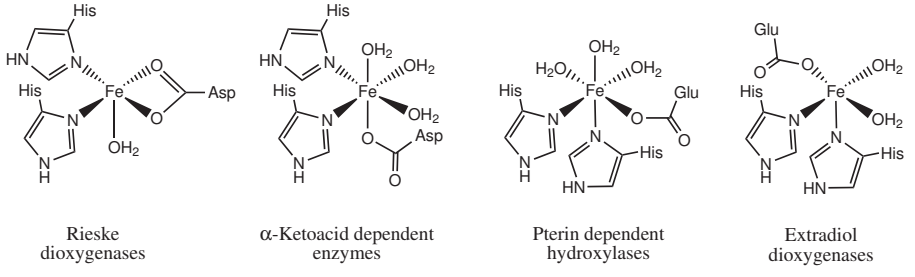

Figure 2.4: *Four different nonheme iron enzyme families using the 2-his-1-carboxylate coordination motif.*

triangular side at the octahedral coordination geometry. This coordination motif is called 2-his-1-carboxylate facial triad [37, 38], see Figure 2.4. This type of nonheme coordination is more flexible than heme coordination, providing neighboring coordination sides for substrates and cofactors, which opens a variety of additional reaction paths. The spectrum of reactions catalyzed by nonheme iron enzymes covers oxidative cyclisation, mono- and dioxygenation, hydroperoxidations and epoxidations [39]. α-Ketoglutarate (αKG) dependent enzymes form the largest family of mononuclear nonheme iron enzymes [39]. The enzymatic cycle of these enzymes has been studied extensively. They use molecular oxygen to generate a highly reactive ferryl-oxo intermediate, which then can act as hydrogen atom abstracting species [40], see Figure 2.5. In the resting state water is coordinated to the iron

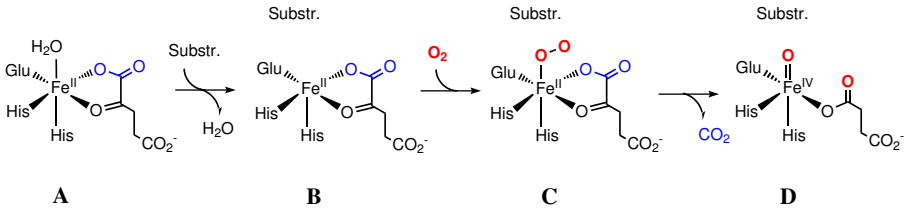

Figure 2.5: *Formation of the highly reactive ferryl-oxo intermediate in αKG-dependent enzymes.*

ion in axial position (**A**). When the substrate enters the active site the water is released (**B**), leaving a free coordination site available for oxygen binding (**C**). Once oxygen has bound to the iron ion, it reacts with the cofactor αKG under heterolytic O-O bond cleavage. This results in decarboxylation of the cofactor, leading to the formation of a highly reactive ferryl-oxo intermediate **D** [41], which is the active species reacting with the substrate.

Halogenases

Among the αKG-dependent nonheme iron enzymes exists a subclass that catalyzes oxidative halogenation rather than the more typical hydroxylation. One of these enzymes, SyrB2[4], shows a variant of the 2-his-1-carboxylate coordination motif, wherein the carboxylate is substituted by a halogen ion [42]. SyrB2 catalyzes the chlorination of threonine within syringomycin E biosynthesis. The proposed mechanism of this oxidative halogenation is given in Figure 2.6. SyrB2 is only active if the threonine is tethered

[4]The name "Syrb2" derives from its participation in Syringomycin E biosynthesis, an antifungal produced by the plant bacterium Pseudomonas syringae.

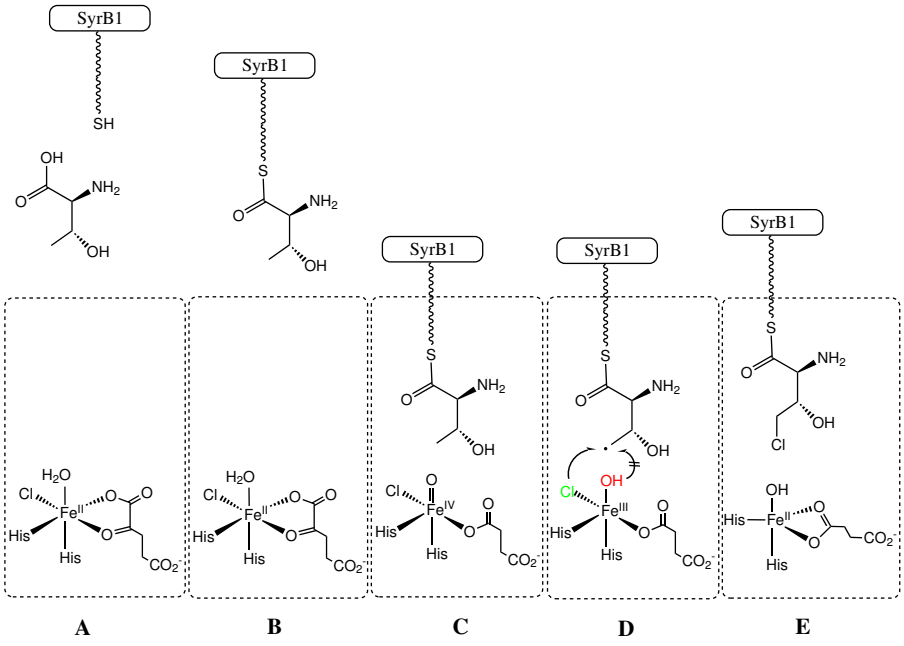

Figure 2.6: *Proposed mechanism for the oxidative chlorination of threonine to 4-Cl-threonine by the αKG-dependent enzyme SyrB2.*

to the thiolation domain of another protein called SyrB1 (**A** to **B**). The substrate is then passed into the active site of SyrB2 through a 17Å long tunnel. After oxygen uptake the reactive iron-oxo species is generated through decarboxylation of the αKG cofactor (**C**). Next a hydrogen atom is abstracted from the methyl group of threonine. The threonyl radical generated during this hydrogen atom abstraction (**D**) could in principle recombine with either hydroxyl or chlorine. However, for this natural substrate only chlorinated products have been observed (**E**). Experimental studies have shown that SyrB2 exhibits hydroxylase activity when presented with alternative substrates tethered to the SyrB1 carrier protein. These findings led to the conclusion that SyrB2 controls the partitioning between halogenation and hydroxylation by substrate positioning [43].

Binuclear Iron Enzymes

As mentioned above, nonheme proteins lack electron buffering ligands. However, one way to reach electronic flexibility is given by the formation of polynuclear complexes with indirect metal-metal interaction [44].

Hemerythrin, a protein involved in O_2 transport of invertebrates[5], has a diiron core in which the two iron centers are bridged by aspartate, glutamate and one hydroxide. Similar bridging can be seen for the R2 unit of ribonucleotide reductase (RNR), an enzyme involved in DNA synthesis, and for the hydroxylase component of soluble methane monooxygenase (sMMO), which catalyzes the conversion of methane to methanol, see Figure 2.7. The

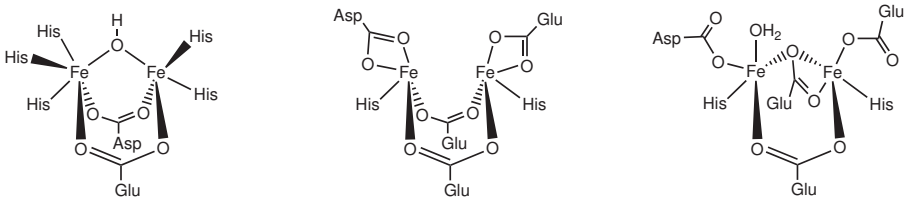

Figure 2.7: *The diiron core in its resting state (reduced form) for the oxygen carrier protein hemerythrin and the enzymes RNR and sMMO.*

bridging atoms of these binuclear iron sites are solely oxygen donors, either originating from the carboxylic function of an amino acid or from water/dioxygen. The key intermediates in the catalytic cycles of MMO and RNR involve high-valent iron-oxo species, see Figure 2.8. MMOH reacts with

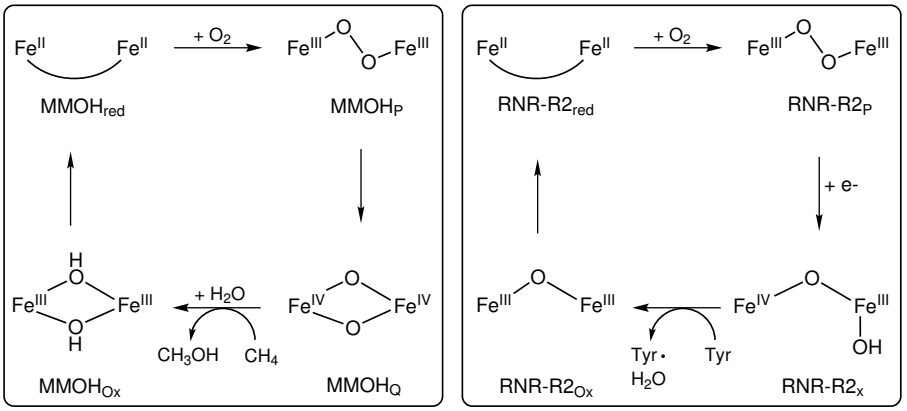

Figure 2.8: *Observed intermediates for the dioxygen activation cycles of sMMO and RNR.*

[5]Invertebrates, i.e. animals without a backbone, form the majority of all animal species. Carl von Linné divided them into insects and worms, however, today there are over 30 phyla, such as molluscs and arthropods.

O_2 to give a peroxo-diiron(III,III) intermediate $MMOH_P$. This intermediate undergoes further transformation into a high-valent diiron(IV,IV) species $MMOH_Q$, which most likely has a $Fe(IV)_2(\mu\text{-}O)_2$ core [45]. This high-valent intermediate is a kinetically competent oxidant for methane [46], which has the strongest C-H bond among all alkanes. The catalytic cycle of the R2 RNR is in many ways similar to that of sMMO. Again, the resting diiron(II,II) state reacts with O_2 by forming a diiron(III,III)-peroxo intermediate. This peroxo species rapidly decomposes into a high-valent intermediate $R2_X$. Unlike $MMOH_Q$, it contains an $Fe(III)(\mu\text{-}O)Fe(IV)$ core. This high-valent iron-oxo species is known to oxidize the phenol group from a tyrosine residue, which in turn yields a tyrosyl radical important for the catalysis.

2.4 Biomimetic Iron Compounds

Understanding the reactivity of such heme and non-heme iron enzymes is an important goal of biomimetic model chemistry. Model compounds are synthesized for different purposes. One approach is the spectroscopic model, where it is implied that the spectroscopic properties of a biochemical system are determined by the first coordination sphere of the metal center. Synthetic models are build to mimic certain structural particularities, e.g. kind and number of bridging atoms. The aim is to reproduce spectroscopic features which allows to draw conclusions about the (uncertain) coordination sphere present in the biochemical archetype. Another approach is functional modeling where the aim is to qualitatively simulate the reactivity of an enzyme. The holy grail of biomimetic chemistry, however, is to quantitatively simulate the reactivity of these enzymes regarding reaction rates and substrate specificity.

Unfortunately, it is hardly possible to mimic the complexity of a protein structure with such low-molecular complexes as they are being used in synthetic chemistry. The protein structure protects the active site, which otherwise might be vulnerable if exposed to the outside. In contrast, it is difficult to protect synthetic compounds from unwanted reactions. A comparison to organometallic chemistry shows that such complexes are very sensitive and demand a careful synthesis and storage. Due to this lack of protection and flexibility many synthetic complexes can only cover certain parts of a full enzymatic cycle and are thus regarded as “partial” models.

Functional Models

The preparation of synthetic model compounds that resemble geometry and reactivity of an enzymes active site is a challenging task for synthetic chemistry. The ligands that are used in the synthesis have to fulfill certain

conditions, e.g. they should be compatible with the different oxidation states of the metal site. Multidentate ligands are preferred because chelation enhances the binding to the metal and furthermore introduces a certain rigidity to the complex. Steric properties of the ligands are of great importance to protect the metal and to govern the state of aggregation, i.e. formation of mono- or polynuclear species [47, 48]. Figure 2.9 shows a few ligands that where successfully used in the synthesis of biomimetic model compounds [49].

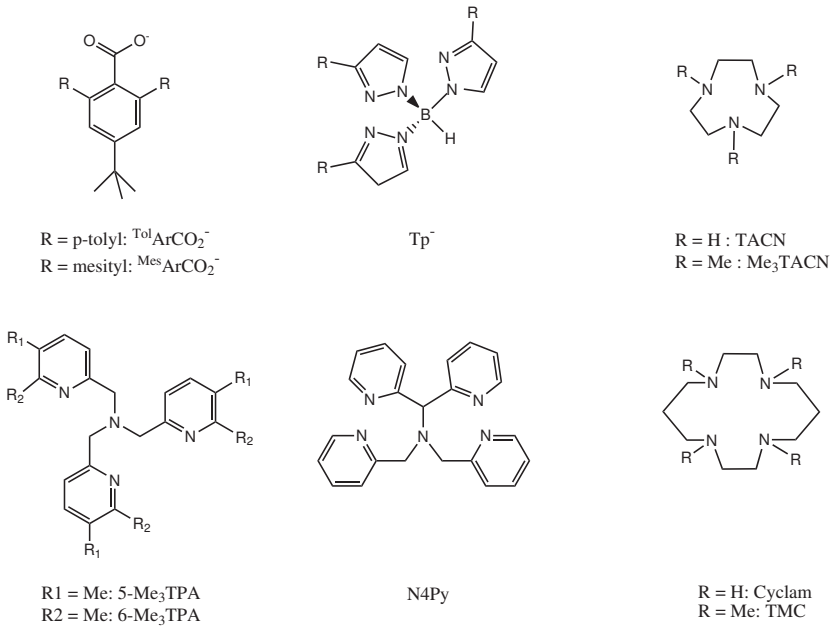

Figure 2.9: *Two-, tri- and tetradentate ligands used to build biomimetic model compounds.*

Most of these ligands bind to the iron atom via nitrogen donor atoms, which does not correspond to the large part of oxygen donors found in the nonheme coordination environment. The reason is that oxygen donating ligands very easily form salts which complicates the synthesis of the corresponding biomimetics. However, the growing number of functional model complexes synthesized from polydentate nitrogen ligands with different topologies, demonstrates the capability of these ligands to support highly oxidized metal centers [50].

A comparison between related tetradentate ligands shows dramatic differences in reactivity depending on the topology of those ligands. It is

important whether the additional ligand coordinating to the iron center after at the remaining coordination site is cis or trans to the oxo-group [51]. One example is given in Figure 2.10 by a comparison of the two tetradentate ligands TPA and TMC[6]. The contrasting effects of cis and trans ligands

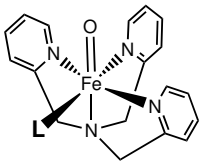

TPA
tetradentate cis-ligand

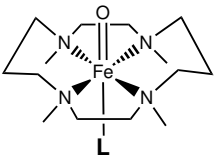

TMC
tetradentate trans-ligand

Figure 2.10: *Two oxoiron(IV) complexes containing a cis-ligand in $[Fe^{IV}(O)(TPA)L]^{2+}$ and a trans-ligand in $[Fe^{IV}(O)(TMC)L]^{2+}$.*

on the reactivity derives from perturbations to the electronic structure of the highly covalent Fe(IV)=O moiety. The Fe=O bond can be described as consisting of a σ bond, formed by the overlap of the empty metal d_{z^2} orbital and the oxygen p_z orbital, and a π bond due to the interactions between the half-filled metal d_{xz} and d_{xy} orbitals and the oxygen p_π orbitals [52, 53]. A ligand trans to the oxo group can exert a large effect on the electronic structure since it can compete with the oxo group by strong interaction with both $d\sigma$ and $d\pi$ orbitals. Weakening of the Fe(IV)=O bond by trans coordination of electron-donating ligands (like the soft base thiolate) leads to a dramatic increase of the hydrogen atom abstraction reactivity of the Fe(IV)=O unit [51]. A cis ligand, on the other hand, can only modulate the Lewis acidity of the Fe=O center, i.e. electron-withdrawing ligands enhance the oxidative power of a iron-oxo unit [51].

Synthesis of binuclear iron complexes that mimic the "diamond-shaped" bis(μ-oxo) motif known from MMO and RNR was only possible by the use of the following two key synthetic strategies. First, to avoid decomposition reactions, solutions and solids had to be handled at low temperature. And second, chelating ligands had to be used, usually with alkyl substituents, to facilitate crystallization and inhibit intermolecular interactions [54].

Figure 2.11 shows the synthesis of first crystallographically characterized bis(μ-oxo)diiron(III,III) complex based on acid/base/aquation chemistry [55]. The precursor complex (**A**) was prepared from Fe(II) salts by tert-butyl hydroperoxide in using 6-Me_3TPA as ligand [56]. Lack of the 6-Me

[6]TPA = tris(2-pyridylmethyl)amine, TMC = 1,4,8,11-tetramethyl-1,4,8,11-tetraazacyclotetradecane.

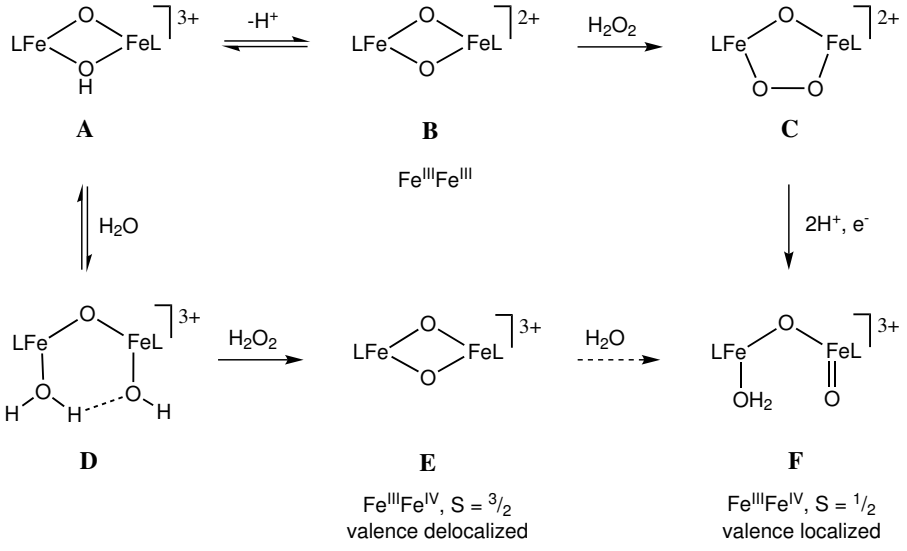

Figure 2.11: *Strategy for the synthesis of different bis(μ-oxo)diiron species.*

substituents gave trinuclear complexes during deprotonation [54]. In the presence of water **A** is converted to **D**. Further reaction with hydrogen peroxide at -40°C[7] leads to the generation of a deep green species **E**, which is best described as valence delocalized, ferromagnetically coupled low-spin Fe(III)/low-spin Fe(IV) pair with an overall S=3/2 ground state. The related diiron(III,IV) complex **F** can be synthesized from **B** via intermediate **C**. In this case the experimental results indicate that it contains a valence localized, antiferromagnetically coupled high-spin Fe(III)/high-spin Fe(IV) pair with an S=1/2 ground state. Its spectral features resemble those of compound $R2_X$ in ribonucleotide reductase [54].

[7] Anders Celsius, 1701–1744, was a Swedish astronomer who proposed a temperature scale based on the freezing and the boiling point of water. In his scale the freezing point of water was set to 100 and the boiling point to zero degree. One of such thermometers can be seen in the Gustavianum in Uppsala.

3

Generation of Adipic Acid

After having presented the biochemistry of iron and biomimetic concepts this chapter introduces the first example of a reaction catalyzed by a biomimetic iron complex. The complex presented here has structural similarity to the active site of heme proteins, i.e. iron(II) is coordinated by a porphyrin. In the presence of oxygen a reactive (Porph)Fe(IV)=O species is formed, that catalyzes the conversion of cyclohexane into adipic acid.

3.1 Introduction

Adipic acid is a key chemical mainly used in the production of polymers, more specifically for nylon, pvc and polyurethane synthesis [57]. Industrially it is synthesized by oxidation of cyclohexane in air over a homogeneous cobalt or manganese catalyst at 150–160°C. This process results in a mixture of cyclohexanol and cyclohexanone referred to as "KA oil" (ketone-alcohol oil). The components of the KA oil are further oxidized using nitric acid, which leads to the generation of nitrogen oxides. Hence, there is considerable interest towards the usage of molecular oxygen or hydrogen peroxide as oxidant, which would provide an environmentally friendly process [58–61].

Experiments reporting on an iron-porphyrin complex able to catalyze the conversion of cyclohexane to adipic acid in the presence of oxygen led to the mechanistic study presented herein. The reaction was conducted at 140°C under 25 atm[1] with cyclohexane as both, solvent and substrate. This "one-

[1]This is done using an autoclave as reaction vessel, that was charged with 25 atm of O_2. Interestingly, a reduced reaction temperature of 130°C led to a dramatic drop in the yield of adipic acid [62], which means that the rate limiting step must have an activation barrier around 23 kcal/mol for a reaction rate of $1s^{-1}$ (compare Figure 1.2).

pot" ansatz requires less energy then conventional methods and moreover, uses molecular oxygen as oxidant [62].

It is well known that (Porph)Fe(II) complexes can bind and cleave O_2 via the formation of a diiron peroxide [63–67]. The mechanistic study presented herein is thus focused on the mechanism of cyclohexane oxidation, starting with the reactive oxoferryl species.

3.2 First Hydroxylation Step

The calculated ground state of the (Porph)Fe(IV)=O reactant complex is a triplet (low-spin configuration on iron), in which one of the unpaired electrons is partially delocalized to the oxo group.

The reaction is initialized by hydrogen atom abstraction from cyclohexane. Hydrogen atom transfer (HAT) can be regarded as proton-coupled electron transfer, in which a proton and an electron are both transferred from the same donor to the same acceptor, more or less simultaneously. During this step the iron ion is reduced, and depending on the spin of the transferred electron there are two possible outcomes. Defining the spin of irons unpaired electrons as α, the multiplicity of the complex will increase if the electron transferred via HAT also carries α-spin. This path results in an intermediate radical complex, with the unpaired electrons on iron antiferromagnetically coupled to the remaining β-spin on the substrate radical. If the transferred electron instead carries β-spin, the number of unpaired electrons on iron will decrease, yielding an intermediate radical complex with ferromagnetic coupling between the unpaired electrons on the iron ion and the substrate radical.

Despite the fact that the ground state of the reactant complex is a triplet, the lowest barrier for the hydrogen atom abstraction is found for high-spin iron in the quintet state, with an barrier of 13.6 kcal/mol. Thus, the system has to undergo a spin crossing before reaching the transition state. A behaviour typical for the reduction of the Fe(IV)=O group in strong ligand fields [29, 53]. The triplet ground state reactant and the transition state for hydrogen atom abstraction are both shown in Figure 3.1

The formation of the intermediate radical complex is endothermic with 6.7 kcal/mol. Radical recombination between the OH ligand on the iron center and the substrate is exothermic by -37.0 kcal/mol for the reactive quintet state. As a reflection of the large exothermicity the barrier for this step only 0.7 kcal/mol higher than the preceding intermediate complex. The final dissociation of cyclohexanol is easy feasible since it is only weakly coordinated to the iron-porphyrin complex (ΔH=1.3 kcal/mol). A summary of the reaction energetics is given in Figure 3.2.

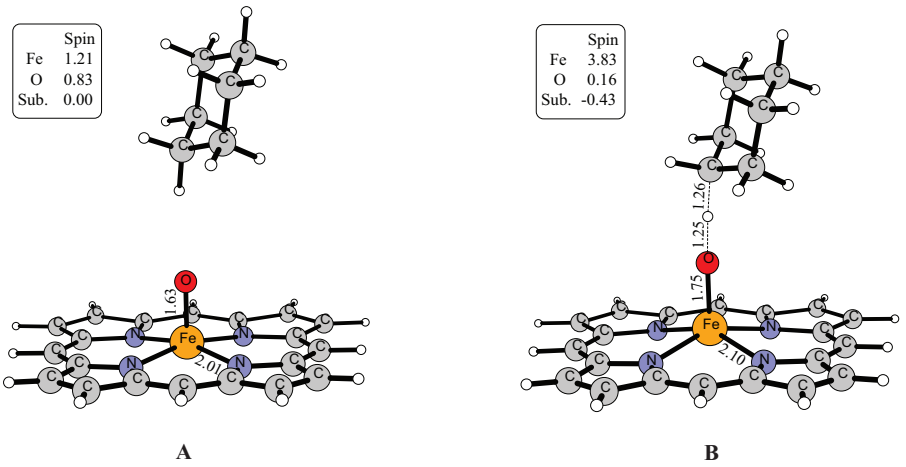

Figure 3.1: A: *The [(Porph)Fe(IV)(O)–(C_6H_{12})] reactant complex in its triplet ground state;* **B**: *Transition state for hydrogen atom abstraction in the quintet state. The most important distances and spin populations are given.*

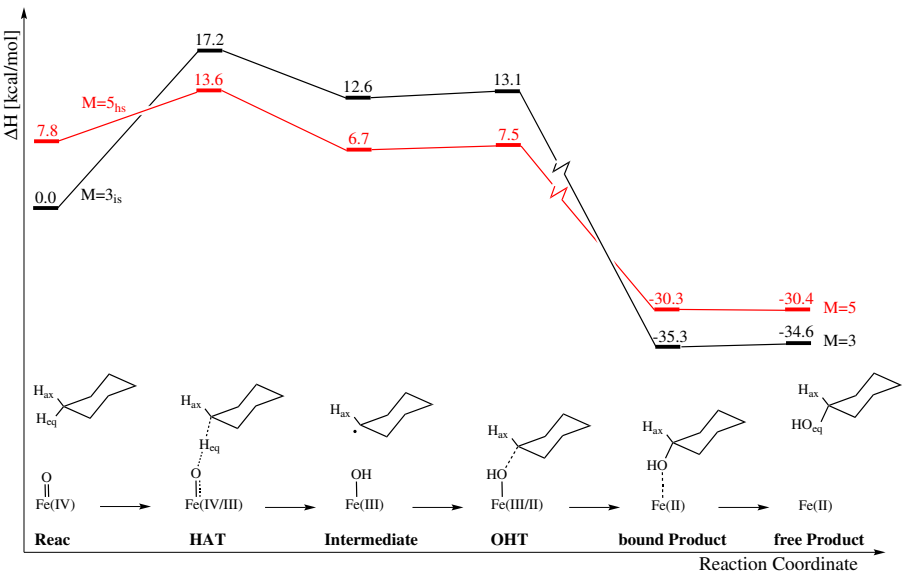

Figure 3.2: *Energy profile for the iron-porphyrin catalyzed oxidation of cyclohexane to cyclohexanol.*

3.3 Second Hydroxylation Step

At the beginning of the second hydroxylation cycle a hydrogen bonded complex is formed between a new (Porph)Fe(IV)=O complex and cylcohexanol (Figure 3.3**A**). This complex is rather stable and lies 8.3 kcal/mol lower than the separated reactants. As for the first hydroxylation step the system undergoes a spin crossing from the triplet ground state of the reactant to the quintet transition state. Starting from the hydrogen bonded complex this hydrogen atom abstraction requires 17.8 kcal/mol, which is 4.2 kcal/mol higher than the previous hydrogen atom abstraction that led to the formation of cyclohexanol. However, if compared to the separated reactants the hydrogen atom abstraction would have a barrier of only 9.5 kcal/mol, which is 4.1 kcal/mol below the previous hydrogen atom abstraction in the first hydroxylation sequence (compare Figure 3.2 and 3.4). The reason for the different barrier heights is due to the hydrogen bond in the reactant complex that on the one hand lowers the reactant state so much, that the barrier effectively increases, but on the other hand also stabilizes the transition state enough to lower it below the barrier for the first HAT in cyclohexanol generation, if compared to the separated reactants. The HAT reaction step is endothermic with 8.6 kcal/mol, leading to a radical intermediate, from which radical recombination has a barrier of only 3.1 kcal/mol.

The resulting cyclohexane-1,2-diol has both neighboring OH-groups in equatorial positions. Two other conformations are possible for ortho-substitution – one of the OH-groups in equatorial, and the other one in axial position, or both OH-groups in axial positions. The di-equatorial conformation was chosen, since it is 1.2 kcal/mol more stable than the equa-axial conformation, and 3.5 kcal/mol more stable than the di-axial conformation.

3.4 C-C Bond Cleavage

A new (Porph)Fe(IV)=O complex forms two hydrogen bonds with the two equatorial OH-groups of cyclohexane-1,2-diol (Figure 3.5 **A**). This hydrogen bonded complex lies only -4.0 kcal/mol below the separated reactants, it has thus only half as large stabilization than the corresponding hydrogen bonded reactant complex in the second hydroxylation step of cyclohexane-1,2-diol generation. This can be explained by the fact that free cyclohexane-1,2-diol has an internal hydrogen bond that is broken upon coordination to (Porph)Fe(IV)=O, which partly cancels the energy gain.

The mechanism sequence for the C-C bond cleavage starts with hydrogen atom transfer from one of the substrates OH-groups to the iron-oxo complex, see Figure 3.5 **B**.

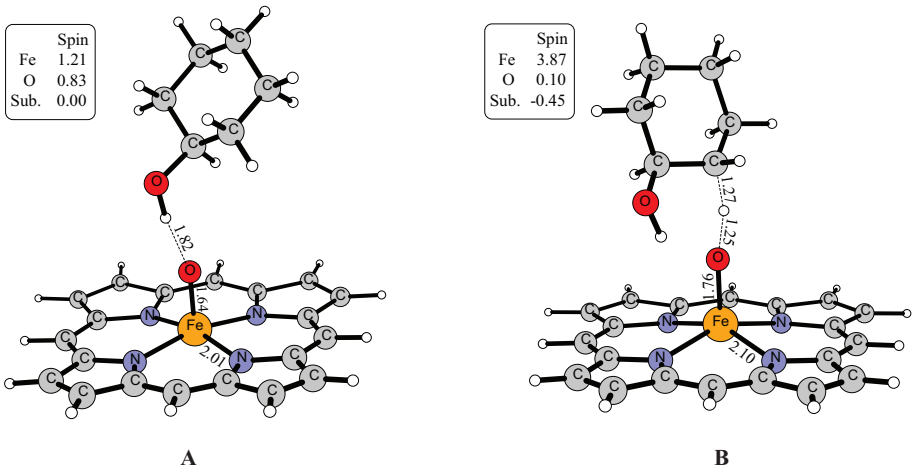

Figure 3.3: A: *The [(Porph)Fe(IV)(O)–($C_6H_{11}OH$)] reactant complex in its triplet ground state;* **B**: *Transition state for HAT in the reactive quintet state. The most important distances and spin populations are given.*

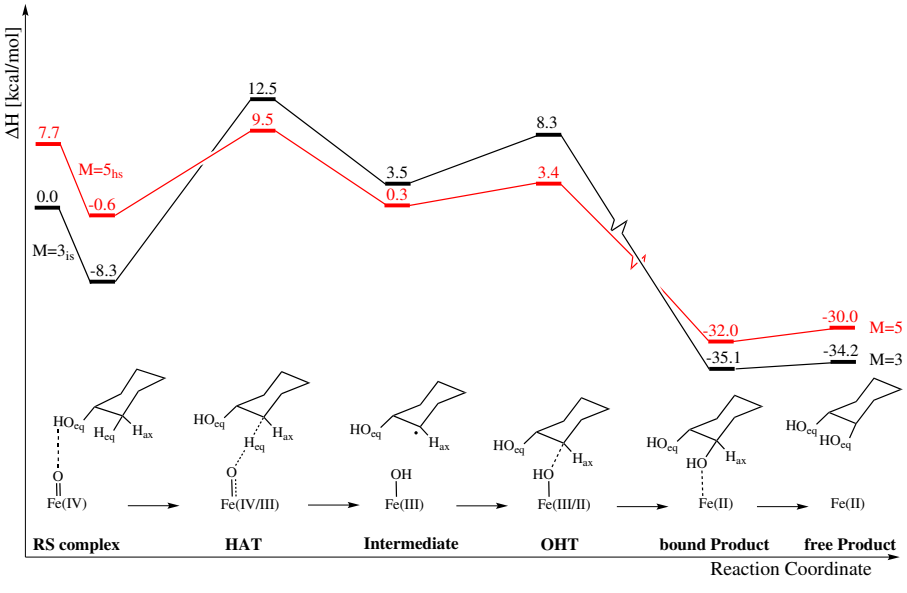

Figure 3.4: *Energy profile for the hydroxylation of cyclohexanol to cyclohexane-1,2-diol.*

This O-H hydrogen atom abstraction is much lower than the previously reported C-H abstraction barriers, with only 10.2 kcal/mol in the reactive quintet state. The radical intermediate formed after this initial hydrogen abstraction (Figure 3.5 **C**) is very unstable in regards to C-C bond dissociation. This C-C bond dissociation is furthermore concerted with a second hydrogen atom abstraction from the remaining hydroxide of the substrate to the (Porph)Fe(III)OH complex (Figure 3.5 **D**).

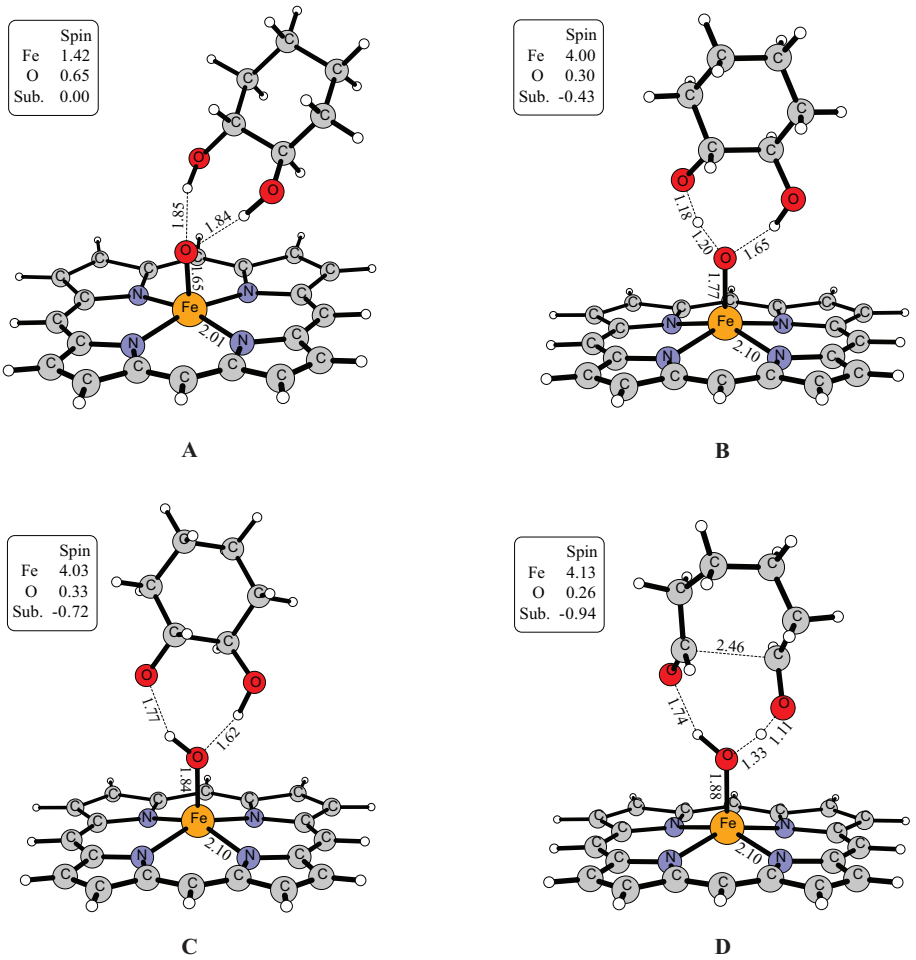

Figure 3.5: **A**: *The reactant complex [(Porph)Fe(IV)(O)–$C_6H_{10}(OH)_2$] in its triplet ground state;* **B**: *Transition state for HAT in the reactive quintet state;* **C**: *Reaction intermediate complex [(Porph)Fe(III)(OH)–$C_6H_{10}(OH)O$] in the reactive quintet state;* **D**: *Concerted transition state for C-C bond cleavage and second HAT in the reactive quintet state.*

In gas-phase, the calculated barrier for this step is very small with only 1.8 kcal/mol. However, when dielectric solvent effects and zero point corrections are added, the energy of the optimized TS is lowered to 5.4 kcal/mol below the radical intermediate. Therefore, it can be concluded that after the initial O-H hydrogen atom abstraction the system proceeds towards the formation of hexane-1,6-dial without further barriers, see Figure 3.6. A more symmetric concerted TS in which both the hydrogens are transferred simultaneously to the iron-oxo group along with the intradiol C-C bond cleavage, was carefully searched for, but could not be located, and therefore does not exist.

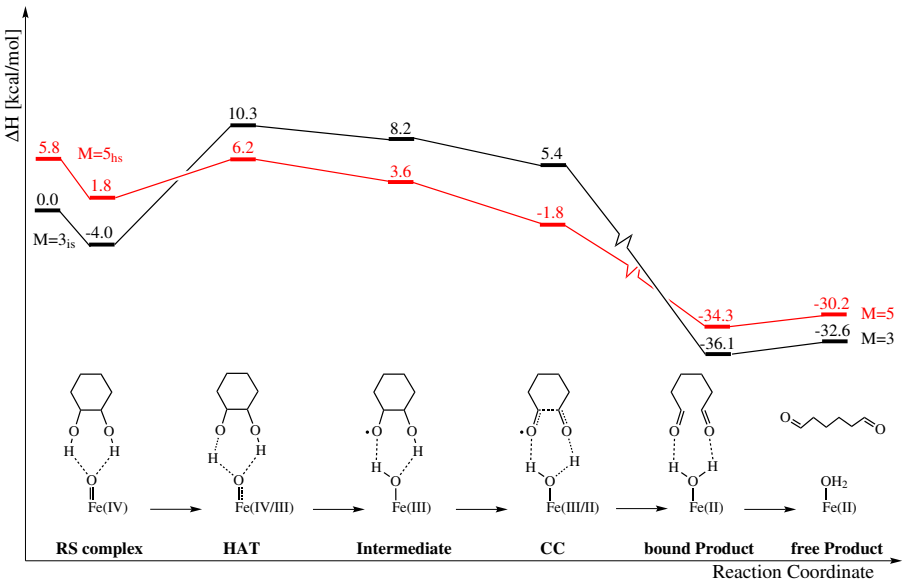

Figure 3.6: *Energy profile for the oxidation of cyclohexane-1,2-diol to 1,6-hexanedial via intradiol C-C cleavage.*

The C-C bond cleavage leads to the formation of adipaldehyde. The remaining steps in the generation of adipic acid consist of two similar, consecutive oxidations of adipaldehydes two aldehyde groups into carboxylic groups. The chemistry involved follows the paradigm of the Fe(IV)O reactivity presented in this chapter. However, in this case hydrogen atom abstraction occurs from a carbonyl, which has a higher stabilization in its radical state than a normal carbon radical. Because of this the hydrogen atom abstraction barriers are much lower than for normal C-H abstraction, and furthermore the formation of the radical intermediate is exergonic. The first hydrogen atom abstraction from adipaldehyde has a barrier of 7.7 kcal/mol in the reactive quintet state. Similarly, the hydrogen atom

abstraction from 6-oxohexaonic acid has a barrier of 8.2 kcal/mol. In both cases the subsequent hydroxylation has a much lower barrier with 3.2 and 1.8 kcal/mol, respectively.

3.5 Conclusions

At the present state the iron catalyzed oxidation of cyclohexane to adipic acid is not very selective. The main by-products formed during the reaction are succinic acid, glutaric acid, cyclohexanol and cyclohexanone [68]. The shorter dicarboxylic acids succinic- and glutaric acid are likely to be formed by over-oxidation of adipic acid, which is difficult to avoid due to the thermodynamic driving force for aliphatic oxidation by the oxoferryl group.

A summary of the complete mechanism beginning with cyclohexane is presented in Figure 3.7. The first transformation in this mechanism involves

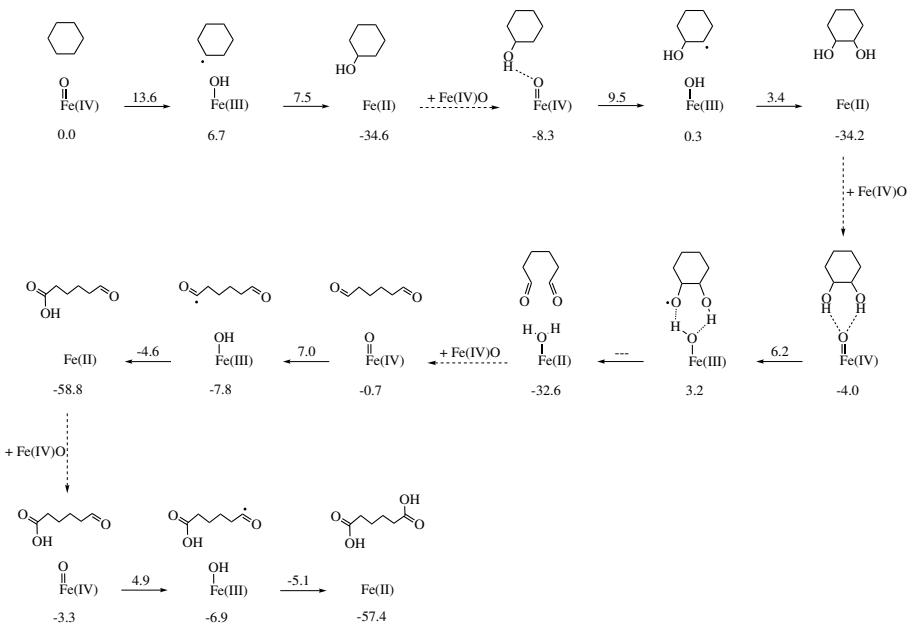

Figure 3.7: *Complete mechanism for the conversion of cyclohexane to adipic acid. Because the thermodynamics for the Fe(IV)O formation are unknown, each of this consecutive series has the separated reactant/substrate species as reference point.*

the formation of cyclohexane-1,2-diol from cyclohexane by two consecutive hydroxylation steps. These hydroxylations occur via hydrogen atom transfer from the substrate to the iron(IV)-oxo complex, followed by re-binding of

the OH-group with the carbon radical. The highest barrier along this path is the second hydrogen atom abstraction with 17.8 kcal/mol. In the next step, cyclohexane-1,2-diol is converted to adipaldehyde by C-C bond cleavage. This is initiated by a hydrogen atom abstraction from one of the substrates OH-groups which has a barrier of 10.2 kcal/mol. The intradiol C-C bond cleavage occurs spontaneously alongside with a second hydrogen atom transfer from the remaining OH group. Finally, the resulting adipaldehyde is oxidized to adipic acid via two consecutive hydrogen abstraction/hydroxylation steps.

The highest calculated barrier along the reaction path of adipic acid formation from cyclohexane is thus the HAT during the second hydroxylation step with 17.8 kcal/mol. This barrier has to be compared to the kinetics of (Porph)Fe(IV)=O generation from (Porph)Fe(II) and O_2, that has been determined experimentally. The measured activation parameters for enthalpy (ΔH_{TS} = 14.5 kcal/mol) and entropy (ΔS_{TS} = -15 cal/mol) amount to a free energy barrier of 17.4 kcal/mol at -80°C [64], which corresponds to a barrier of 20.7 kcal/mol at 140°C. These results indicate that the rate limiting step in the oxidation of cyclohexane to adipic acid might not the substrate oxidation itself, but rather the generation of the (Porph)Fe(IV)=O oxidant. This aspect is interesting because it is known that the generation of the (Porph)Fe(IV)=O from (Porph)Fe(II) and O_2, is significantly faster when a coordinating Lewis base is added to the reaction solution [67]. This in turn would make it possible to run the reaction at lower temperature, which could have positive effects on the selectivity.

4

Catechol Cleavage

The enzymatic ring-cleavage of catechol derivatives (1,2-dihydroxybenzene) is catalyzed by two groups of enzymes, extra- and intradiol cleaving dioxygenases. The aim is to understand the factors that lead to either extradiol cleavage, resulting in 2-hydroxymuconaldehyde, or intradiol cleavage resulting in muconic acid. The two groups of enzymes differ in the oxidation state of the iron ion and have a different ligand coordination, yet they both involve a common peroxy intermediate in their catalytic cycle. Well characterized model compounds that mimic the functionality of these enzymes offer a basis for direct comparison to theoretical results. The biomimetic complex presented here is known to selectively catalyze the intradiol ring opening of catecholate. An investigation of the detailed mechanism can thus provide an understanding for the factors leading to this observed selectivity.

4.1 Introduction

Before presenting the biomimetic complex the enzymatic mechanism is explained first. Extradiol dioxygenases contain Fe(II) in octahedral coordination by a 2-his-1-carboxylate facial triad [37] and water solvent molecules. In this coordination mode the iron center is exposed to a weak ligand field that leads to a high-spin quintet ground state. The catechol substrate binds directly to the iron ion by replacing the solvent molecules. The reaction is initialized by a binding of the monoanionic substrate, which causes a change in the ligation of the iron atom (see Figure 4.1, step **1**). In the next step dioxygen binds to the iron ion and is reduced to a superoxide, which leads to a partial one-electron oxidation of the substrate. During the further course of the reaction a bridging alkyl-peroxide species

is formed [69, 70] (step **2**). Protonation of this species leads to O-O bond cleavage and the insertion of one oxygen into the catechol ring [71] (step **3**). Final hydrolysis of the lactone intermediate by the remaining hydroxide results in product release (step **4**).

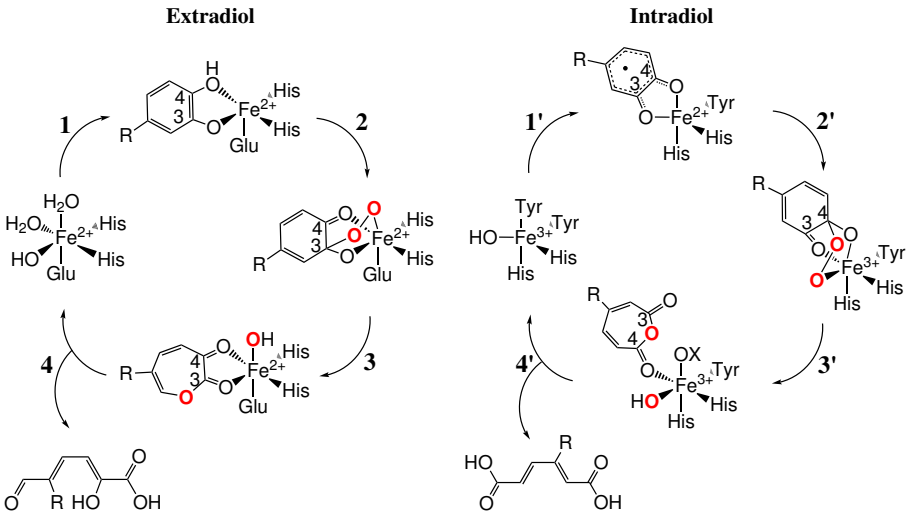

Figure 4.1: *Proposed catalytic cycles for extra- and intradiol cleaving dioxygenases.*

Intradiol dioxygenases cleave the ring between two adjacent hydroxyl substituents. In the resting state iron(III) is coordinated by two histidines, two tyrosines and a hydroxide. After deprotonation of of its two alcohol groups by first shell ligands, the dianionic catcholate binds to the iron center and is one electron oxidized, which results in an Fe(II)-semiquinone species (Figure 4.1, step **1'**). Dioxygen binds to the metal and subsequently attacks the substrate to form a bridging peroxide (step **2'**). Concerted O-O bond heterolysis and O→C attack (Criegee[1] rearrangement) lead to C-C bond cleavage and insertion of the attacking oxygen into the ring (step **3'**). This step is facilitated by protonation of the bridging peroxide, occurring if a water molecule or a proton donating first shell ligand coordinate to the iron. Nucleophilic attack of the remaining hydroxide yields the final product cic,cis-muconic acid (step **4'**). In contrast to this proposal computational results on intradiol cleaving dioxygenases point in the majority to a homolytic O-O bond cleavage [71, 73–75]. Only in one case a heterolytic

[1]Rudolf Criegee, 1902–1975, was a German chemist. His research on cyclic reactions and rearrangements led him to mechanistic conclusions that were similar to the Woodward-Hoffman rules [72].

Criegee rearrangement could be obtained [75]. However, the energetic difference between homolytic and the heterolytic cleavage is very small (ca. 2 kcal/mol), therefore it is not possible to say which would be more favorable.

Although much is known about each class of enzymes, the factors that determine intra- versus extradiol specificity are still under debate. In a study on biomimetic iron compounds with a series of different ligands it was found that the reactivity of the complex correlates with the Lewis acidity of the iron(III) center [76]. Another model complex with a coordination environment similar to those of the enzymes (two nitrogen and one oxygen donor) was found to have no product specificity [77].

The model complex investigated here is an iron(III) complex in which the iron center is coordinated by a rather stiff tetradentate ligand. Two adjacent coordination sites are available for the binding of catechol which is oxidized to a semiquinone (see Figure 4.2, **R1**). This iron complex can activate dioxygen at room temperature to oxidize catechol exclusively to mucon acid anhydride. The experimentally determined velocity constant for the substrate catechol of 2.77 x 10^{-3} $M^{-1}s^{-1}$ corresponds to an activation barrier of 21.0 kcal/mol [78]. In comparison, the rate constant for intradiol cleaving catechol dioxygenase is k = 2.5 x 10^{5} $M^{-1}s^{-1}$ corresponding to a barrier of 10.1 kcal/mol [79]. Binding

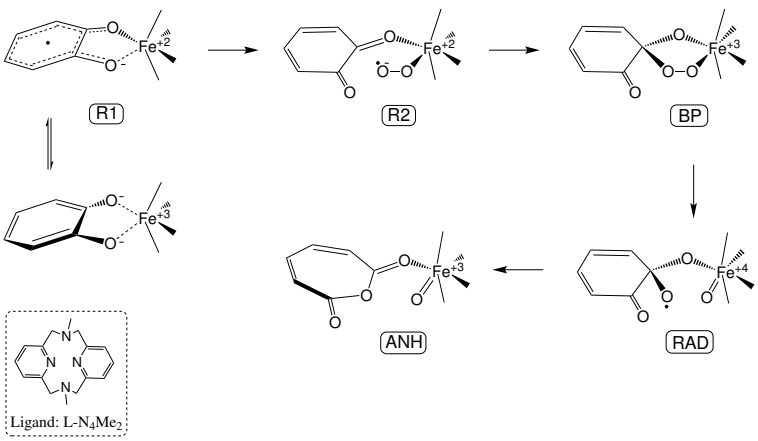

Figure 4.2: *Calculated mechanism for intradiol cleavage catalyzed by the iron(III)(L-N_4Me_2) complex.*

of dioxygen requires partial dissociation of the substrate to provide a free coordination site. The formation of the superoxide leads to further oxidation of the substrate (**R2**). Oxygen subsequently attacks the substrate and forms a bridging peroxide (**BP**). The O-O bond is cleaved homolytically, resulting in a radical state (**RAD**) that decays into the intradiol product (**ANH**).

4.2 Dioxygen Binding

The open-shell nature of iron(III) gives rise to three different spin states – sextet (spin 5/2), quartet (spin 3/2) and doublet (spin 1/2). Furthermore, if the reduction of the iron ion by the substrate is considered, then a total number of 8 spin states exist for **R1**. From X-ray experiments this complex is predicted to be high-spin (S=5/2) based on the bond lengths commonly observed in high-spin complexes with this ligand [78]. The calculated ground state of the reactant differs depending on the density functional used. For B3LYP the calculations agree with experiments. However, if the amount of exact Hartree-Fock exchange is lowered to 15% (B3LYP*), low spin states are slightly preferred (by only 1 kcal/mol). A reactant state involving Fe(III) and unoxidized substrate was found to be high for both functionals, and is thus unlikely to be involved in the reaction.

The dominating ferrous-semiquinonate resonance is very important for the oxygen binding as it directs dioxygen directly to the metal. One oxygen atom of the substrate has to dissociate from the metal ion upon oxygen binding to provide the necessary coordination site, the model complex is shown in Figure 4.3 **B**. The formation of the oxygen adduct **R2** is accompanied by one electron reduction of the dioxygen molecule to a superoxide O_2^-. The electron is provided by the substrate radical, which in turn becomes a neutral quinone. The superoxide complex **R2** has two close

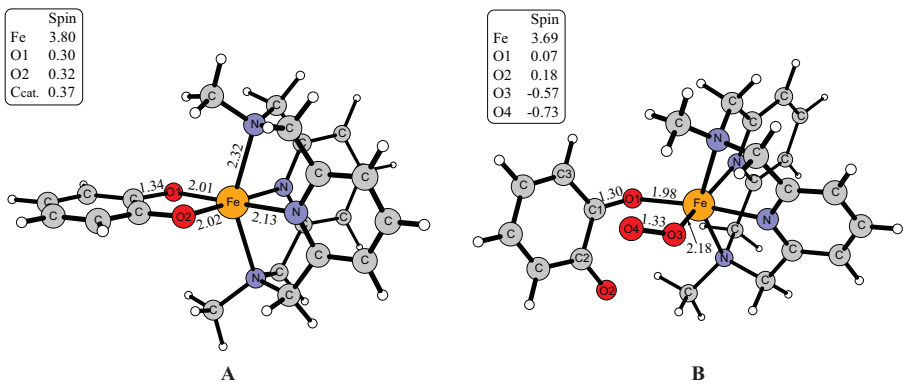

Figure 4.3: A: *The reactant* ^{6}**R1** *in its high-spin ground state* (4α1α); **B**: *The superoxide complex* ^{4}**R2**.

lying spin states, a quartet and sextet state resulting from antiferromagnetic or ferromagnetic coupling between the unpaired electrons of the iron ion and the oxygen center. The quartet state lies at 18.0 and the sextet state at 18.2 kcal/mol relative to the reaction zero level. This energy of the oxygen

adduct is relatively high which might be due to energy required to dissociate one of the substrate oxygens from the iron ion. The oxygen binding was therefore investigated using a computational test-model that includes a protonated triethylamine[2] $[NH(Et)_3]^+$, see Figure 4.4. Upon coordination of the $[NH(Et)_3]^+$ to one of the substrate oxygens dissociation becomes accessible and requires an energy of 13.0 kcal/mol. Subsequent oxygen binding to the free coordination site then only requires 3.7 kcal/mol free energy.

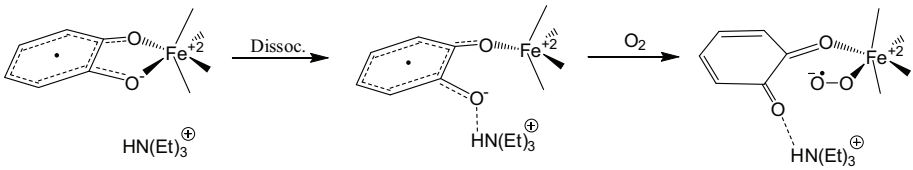

Figure 4.4: *Dissociation of one catecholate bond to provide a coordination site for dioxygen is supported by triethylamine.*

Thus, in total oxygen binding requires an activation barrier of 16.7 kcal/mol in the presence of the base triethylamine. This shows that most of the energy needed to form the oxygen bound adduct **R2** is due to the dissociation of the semiquinonate. Complexes, in which oxygen directly binds to the substrate are found to be 8 to 12 kcal/mol higher than the corresponding metal-bound structures, which is thus unlikely to happen.

4.3 C-C Bond Cleavage

The superoxide of the **R2** complex attacks the aromatic ring of the substrate and forms a bridging peroxide ^{4}**BP**. The electron needed for this reduction is provided by iron ion, which thus is oxidized to Fe(III). The transition state for the formation of the bridging peroxide lies at 23.3 kcal/mol on the quartet potential energy surface and the reaction itself is slightly exergonic with ΔG =-4.5 kcal/mol, the energetic profile for this reaction is given in Figure 4.5. In the next step, the bridging peroxide ^{4}**BP** cleaves the O-O bond homolytically over an barrier of 8.0 kcal/mol. This leads to the formation of a radical state ^{4}**RAD**, best described as an Fe(IV)-oxo species containing an alkoxy radical on the substrate.

The same kind of alkoxy-radical intermediate was also found in previous studies on extra- and intradiol dioxygenases (Fe- and Mn-dependent) [71,74,

[2]The base triethylamine was present in the experimental setup [78]

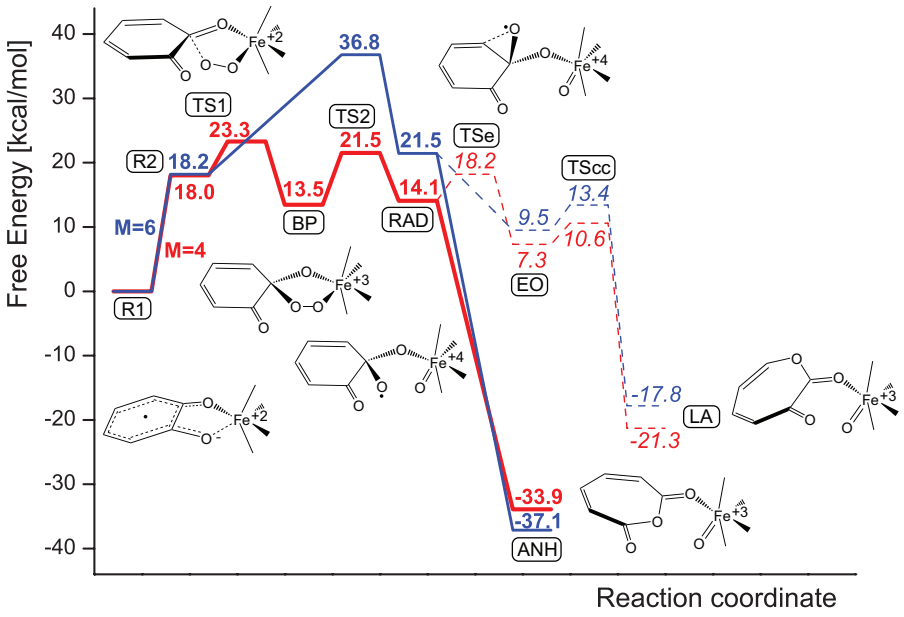

Figure 4.5: *Calculated energy profile along the reaction coordinate: red – quartet state PES, blue – sextet state PES. The solid line represents the intradiol reaction path, the dashed line shows the alternative extradiol reaction path.*

75,80] and homogentisate dioxygenase [73]. In all these cases this short-lived radical intermediate spontaneously converts into the next intermediate.

On the sextet potential energy surface the superoxide complex ^{4}**R2** directly undergoes a homolytic O-O bond cleavage upon attack of the oxygen on the substrate. Therefore no bridging peroxide is formed and the reaction leads directly to the Fe(IV)-oxo/alkoxy radical. However, the transition state for this process lies about 15.0 kcal/mol above the corresponding transition state for O-O bond homolysis. This clearly indicates that the quartet path, going through a peroxy intermediate, is the preferred one for the reaction.

The Fe(IV)-oxo/alkoxy radical ^{4}**RAD** plays a pivotal role for the intra- vs. extradiol cleavage selectivity. On the intradiol path the reaction proceeds in a single step via concerted oxygen attack on the carbon and C-C bond cleavage. Within the computational accuracy no barrier could be found for this step. The homolytic O-O bond cleavage leads thus directly to the formation of complex bound muconic anhydride, which is the final product within the scope of this investigation. During the product formation the system undergoes a spin crossing back to the sextet potential energy surface. In contrast, the alternative reaction of extradiol cleavage proceeds via two

small barriers. The first barrier of 4.1 kcal/mol leads to the formation of an epoxide **EO**, and the second barrier of 3.3 kcal/mol is due to the extradiol C-C bond cleavage.

The biomimetic model complex investigated here differentiates between intra- and extradiol cleavage, because there are additional barriers involved on the extradiol path. Similar results were obtained in previous theoretical investigations, where it was found that the radical intermediate attacks one specific carbon atom spontaneously, whereas attack on the other carbon involves a barrier of 3–4 kcal/mol [71,73–75,80].

4.4 Selectivity

The preferred reaction channel which may lead either to *intra* or *extra* cleavage involves the carbon atom for which the C-C-O-O dihedral angle is closer to 180 degrees. As shown in Figure 4.6 **B**, it is the carbon C2, which is placed in the reactive position with the C2-C1-O4-O3 dihedral amounting to 143.5 degrees, and thus the attack on C2 is barrierless. This geometric

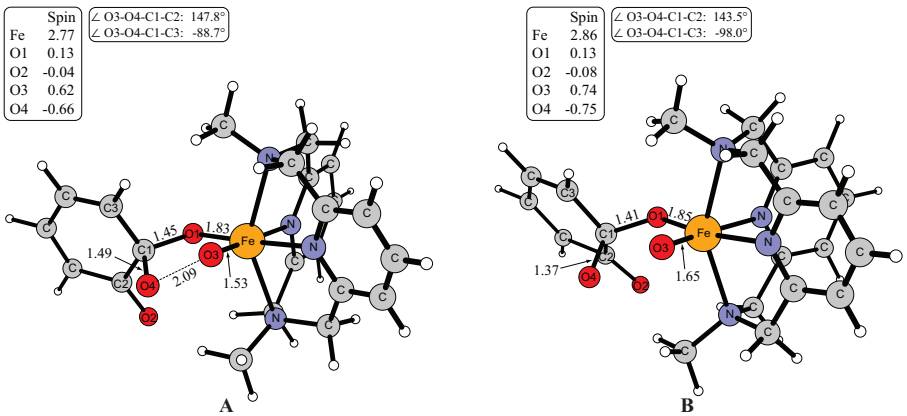

Figure 4.6: A: *Transition state for the homolytic O-O bond cleavage* ^{4}**TS2**; **B**: *The alkoxy radical,* ^{4}***RAD***, formed after the O-O bond cleavage.*

preference might have its roots in the fact that the singly occupied orbital on the oxygen atom (O4) evolves from the σ^* O-O orbital and it remains oriented along the O-O vector even when the O-O bond is broken. Thus, the C-C-O-O dihedral angle close to 180 degrees guarantees a good overlap of the C-C σ and singly occupied O-2p orbital, and hence a spontaneous reaction. The attack on the other carbon (C3) requires reorienting the oxygen 2p orbitals so that the singly occupied orbital interacts with the target carbon,

whereas the doubly occupied one points towards the oxo iron ligand. This reorientation is most likely responsible for the 3–4 kcal/mol barrier.

This preference for in-plane arrangement of the C-C and O-O vectors is much less strict than for the heterolytic Criegee rearrangement because in the radical process the O-O bond breaking and the attack on the carbon are sequential, whereas in the heterolytic reaction these two steps are concerted. Criegee rearrangement has a stringent requirement for in-plane orientation of the two oxygen atoms and the two carbon atoms involved in bond cleavage and formation [75]. Hence, the dihedral angle around 140 degrees determines the chemoselectivity of the radical process, yet it deviates too much for a heterolytic Criegee rearrangement.

4.5 Conclusions

The involvement of a peroxo intermediate in both intra- and extradiol pathways is supported by a number of computational studies [71, 75, 80, 81] and by recent experimental studies of Kovaleva et al. [69, 70], where such an intermediate was actually detected. The reason for the experimentally observed intradiol specificity of the biomimetic complex can be found in the relative orientation of the substrate towards the bridging peroxide, or more precisely in the C-C-O-O dihedral angle. The orientation of the antibonding σ^* O-O orbital towards the target C in the bridging peroxide leads the system directly to intradiol cleavage upon homolytic cleavage of the O-O bond. The alternative path of extradiol cleavage needs to cross a small barrier of 4.1 kcal/mol mainly due to reorientation of the singly occupied O(2p) orbital. The outcome of the reaction can thus be governed by steric restrictions posed on the substrate and the bridging peroxide, this way changing their relative orientation towards each other.

From these results it can be understood how second shell histidine residues involved in the reaction in enzymes can govern the outcome of the reaction. By stabilizing or protonating the bridging peroxide, its orientation towards one of the two possible target carbons can be changed, which preselects the reaction path that follows after O-O bond breakage. This is supported by findings that the selectivity of an extradiol cleaving enzyme was altered to intradiol cleavage upon mutation of a histidine residue involved in the reaction, or upon providing alternative substrates [82].

It is worth to compare the reaction of this biomimetic complex with calculations on an intradiol cleaving enzyme, Protocatechuate 3,4-dioxygenase (3,4–PCD), in which oxygen insertion and C-C bond breakage occur via Criegee rearrangement [75]. The mechanisms starts out very similar, dioxygen is bound as superoxide followed by the formation of a

bridging peroxo intermediate. However, one difference is that the formation of the superoxide **R2** is endergonic for the biomimetic complex. The reason for that is that the binding of the O_2 molecule requires dissociation of one of the substrate oxygens from iron, which was found to be expensive in terms of free energy. The enzymatic environment on the other hand, provides a free coordination site for dioxygen in the beginning of the reaction.

The rate limiting step for the biomimetic complex is the formation of the bridging peroxide, with an activation barrier of 23.3 kcal/mol. For the enzyme, O-O bond cleavage determines the overall reaction rate with an calculated activation barrier of 20.8 kcal/mol. The possibility of the enzyme to facilitate conformational changes through stabilizing interactions with second-shell residues allows for Criegee rearrangement, in which the two oxygen atoms and the two carbon atoms involved have to be oriented in plane. A second requirement for this type of rearrangement is the protonation of the bridging peroxo group. The peroxo group in the biomimetic model, on the other hand, does not bear a proton. Moreover, the rigid ligand on the iron ion does not provide enough flexibility to reach a dihedral C-C-O-O angle of 180 degree and therefore the O-O bond is cleaved homolytically.

5

Chlorination versus Hydroxylation

There exist many natural products featuring carbon-halogen bonds. Vancomycin, chlortetracycline and chloramphenicol have, for example, even substantial therapeutic significance. Enzymes governing incorporation of halogens into unsaturated and aromatic hydrocarbons have been known for some time. Enzymes capable of catalyzing halogenation of unreactive aliphatic compounds, however, have only recently been discovered [83]. These halogenases belong to the α-ketoglutarate dependent group of enzymes presented in chapter 2. The iron(II) ion is coordinated by a 2-his-1-carboxylate facial triad motif in which the carboxylate is replaced by a halogen. An experimentally well studied enzyme, called *SyrB2*, performs exclusive chlorination of the γ-carbon of L-Thr, a process involved in the biosynthesis of the antibiotic syringomycin E [84]. Because hydroxylation of the substrate seems also possible in the proposed mechanism, a key question concerns the origin of the product specificity in halogenases, i.e. why is the chlorination preferred over hydroxylation.

First, the enzymatic mechanism will be discussed. In the second part of this chapter a biomimetic model complex will be presented that, in analogy to the enzyme, catalyzes oxidative chlorination of an unactivated substrate.

5.1 Introduction

Understanding the mechanism by which αKDH incorporate a halogen atom into an unreactive compound is of general interest, because analogous industrial process often require environmentally unfriendly reagents and suffer from low product specificity [85].

5 Chlorination versus Hydroxylation

αKG-dependent halogenases are closely related to αKG-dependent hydroxylases, whose general catalytic mechanism is relatively well understood [86, 87]. As shown in chapter 2 the key-reactive intermediate is a high spin oxoferryl species. An analogous Fe(IV)=O species was observed for the halogenases CytC3 [88,89] and SyrB2 [90], which supports the hypothesis that halogenases and hydroxylases have similar catalytic mechanisms. On the basis of the experimental findings the mechanism presented in Scheme 5.1 was proposed [42]. The catalytic cycle starts with the resting state where Cl

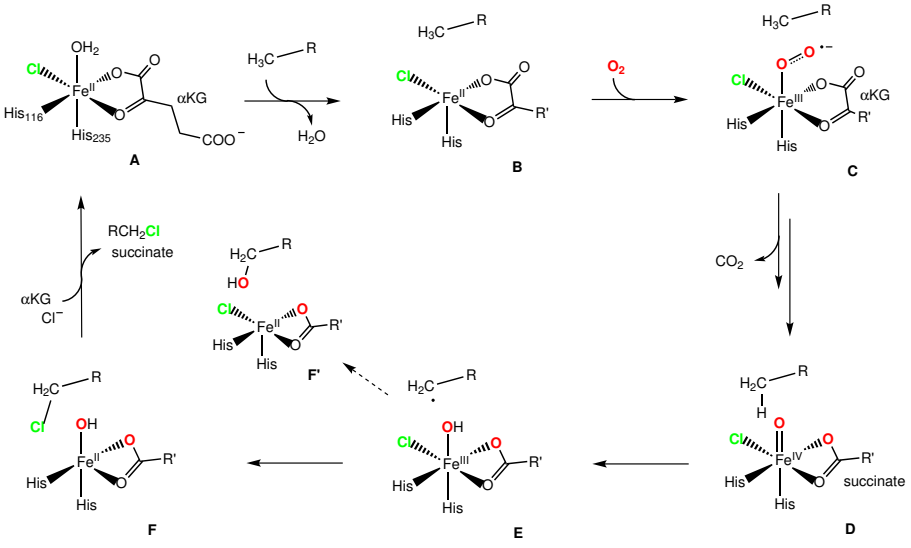

Figure 5.1: *SyrB2 reaction mechanism as deduced from experimental findings.*

and αKG are already bound to iron(II) center **A**. Binding of the substrate is supposed to displace the water ligand and open a coordination site for dioxygen **B**, as was demonstrated for αKG-dependent hydroxylases [91, 92]. Subsequent steps involve dioxygen binding **C** and oxidative decarboxylation of the cofactor **D**. The high-spin oxoferryl species **D** was identified with Mössbauer[1] and EXAFS methods [88–90]. This reactive intermediate is responsible for C-H bond cleavage (**D** → **E**). The carbon-centered radical present in **E** preferentially reacts with the chloro ligand **F**. The typical reaction of αKG-dependent hydroxylases is different at this point, since it involves a rebound of the OH ligand yielding the hydroxylation product **F′**.

[1] Rudolf Mössbauer, born 1929, is a German physicist who received the Nobel prize in 1961 for his discovery of the Mössbauer effect.

Crystal structures currently available correspond to the native states of SyrB2, yet without the substrate (Thr-phosphopantetheine-SyrB1) bound. For this reason, a macromolecular model of the Michaelis complex was constructed and used to model the substrate docking. Based on this structure, a smaller model was constructed, comprising the first- and some of the second shell residues of the iron center. Side chains and model substrate were fixed at the positions marked with asterisks in Figure 5.2.

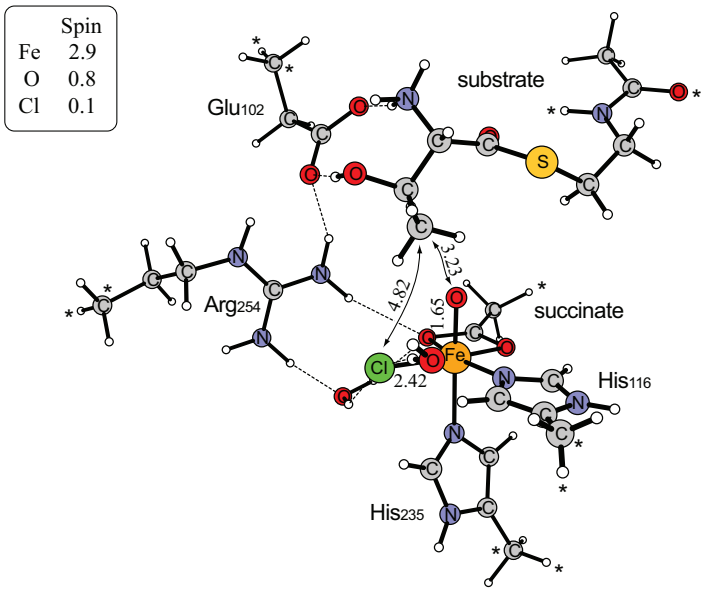

Figure 5.2: *The active site model for the oxoferryl species–substrate complex. Atoms marked with asterisks were fixed.*

5.2 Two Isomers for ClFe(IV)=O

Mössbauer spectra indicate that the reactive oxoferryl intermediate is a mixture of two high-spin Fe(IV) species existing in rapid equilibrium [88,90], which could be of relevance for the mechanism [93]. Swapping of the chloro and the oxo ligand would be much easier in the presence of an empty coordination site than in the coordinatively saturated complex, since an empty place could act as temporary storage. Such an empty coordination site can be formed trans to His116 by a change in the binding mode of succinate from bidentate to monodentate. A plausible mechanism for a conformational change employing this site is presented in Figure 5.3.

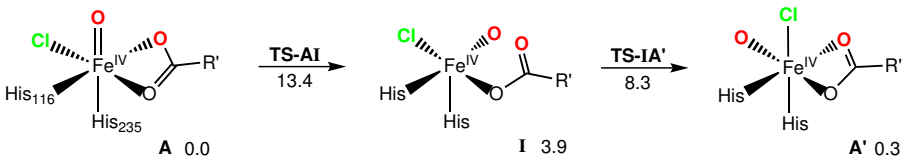

Figure 5.3: *One plausible mechanism for the conformational change of the Cl-Fe(IV)=O species.*

In the first step (**A** → **I**) the oxo ligand moves from the original place to the site *trans* to His116, which involves an activation barrier of 13.4 kcal/mol. The intermediate **I** is 3.9 kcal/mol less stable than **A**, and it features an empty coordination site *trans* to His235. The second step is a concerted, yet asynchronous, transfer of the chloro ligand to the site *trans* to His235, and movement of the oxo ligand to the site initially occupied by the chloride. The calculated energy required for this step amounts to 8.3 kcal/mol.

It should be noted that the calculated Mössbauer spectra for **A** and **A′** fit very well to the experimental data, which validates the proposal that **A** and **A′** represent the two species observed in the experiments.

5.3 Mechanism of the Enzyme

The assumption that two oxoferryl species participate in the reaction makes it possible to formulate a mechanism that reproduces the chlorinating activity, see Figure 5.4. The hydrogen atom abstraction by isomer **A** has a calculated barrier of 18.4 kcal/mol. The radical intermediate **B** produced in this step lies 7.3 kcal/mol above the reactant. Subsequent rebound of the OH ligand involves a barrier of only 0.9 kcal/mol and leads to the hydroxylated product **D** (alcohol). The alternative rebound of the chloro ligand has a barrier of 10 kcal/mol. The chlorination product **C** is furthermore less stable than the alcohol **D**. However, the reverse reaction (**C** → **B**) would involve a barrier of 26.6 kcal/mol and would thus be slower that the catalytic cycle. Therefore, chloride rebound, like hydroxyl rebound, can be considered to be irreversible.

For the stereoisomer **A′** the C-H bond cleavage proceeds through an activation barrier of 17.7 kcal/mol, which is slightly lower than for **A**. The formation of the radical intermediate is almost thermoneutral. The subsequent radical rebound involves a barrier of 5.3 kcal/mol for the axial chloro ligand, as compared to 8.7 kcal/mol for the hydroxide.

Both stereoisomers **A** and **A′** can in principle be active in C-H bond activation. Once the ClFe(III)(OH)/radical intermediate is formed, it decays via rebound of the ligand bound in axial position, i.e. trans to His235, which

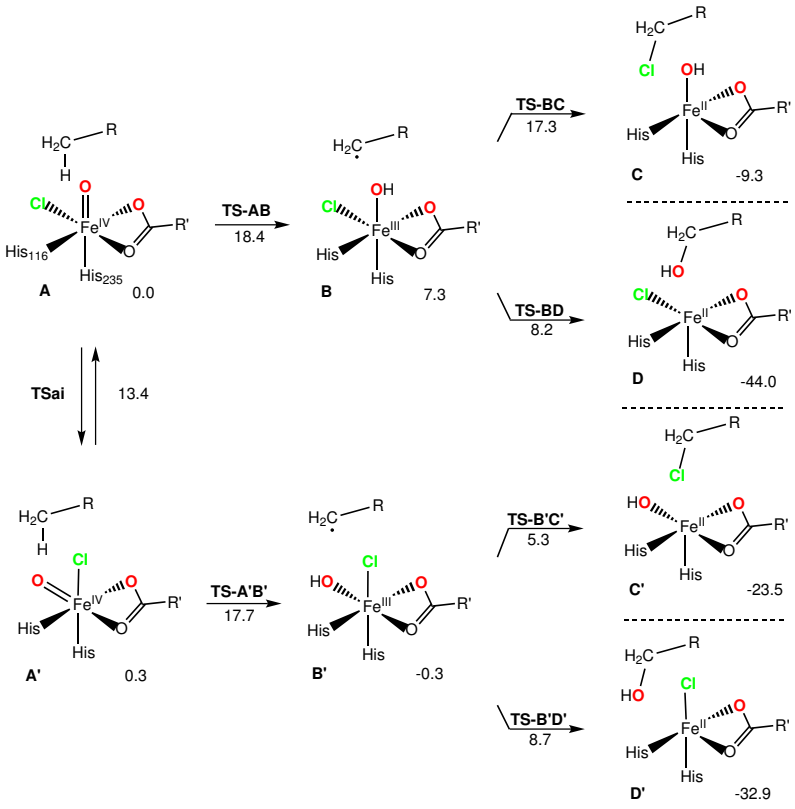

Figure 5.4: *Calculated reaction mechanism for chlorination and hydroxylation of L-Thr by SyrB2. Relative energies given in kcal/mol.*

is due to the orientation of the substrate above the active site. Which of the two isomers participates in the reaction is controlled by the difference in barrier heights for the C-H cleavage performed by the two oxoferryl species **A** and **A'**.

The transition state for hydrogen atom abstraction lies energetically lower for **A'** than **A**, which is surprising if one takes the geometrical structure of the two oxoferryl species into account (Figure 5.5). A shorter distance between the target carbon and the oxo ligand in **A** compared to **A'** should favor C-H bond activation in the "classical" arrangement, i.e. **A**. However, the geometric disadvantage is compensated by factors that stabilize **B'** with respect to **B** by 7.6 kcal/mol. This large stabilization comes from two hydrogen bonds formed between the hydroxide ligand on iron center and two waters present in the active site. These stabilizing factors are to a large extent already

expressed at the transition state structure, as can be seen in Figure 5.5.

Consequence of the exchange of coordination sites between the chloro and (hydr)oxo ligands is a change of chemoselectivity of the reaction. In **B'** the chloro ligand is placed rather close to the radical carbon (3.64Å), whereas the OH is farther away (5.05Å) and interacting with the two waters. As a result, the calculated barriers for Cl- and OH-rebound amount to 5.6 and 9.0 kcal/mol, which leads to chlorination of the substrate.

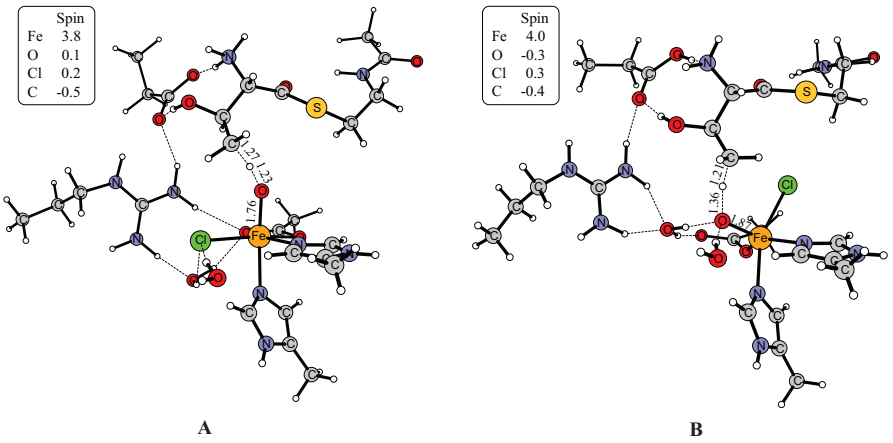

Figure 5.5: *Optimized structures for the two C-H cleavage transition states.* **A***:* **TS-AB** *and* **B***:* **TS-A'B'***.*

5.4 Mechanism of the Biomimetic

The mononuclear iron complex introduced here has a coordination similar to the oxoferryl species of the enzyme SyrB2, with the chloride in cis position to the oxo group. But moreover, in analogy to the enzyme the reaction of the biomimetic with cyclohexane or adamantane exclusively yields the chlorinated product [94]. Since the reactive oxoferryl species is formed in situ from $[(TPA)Fe(III)Cl_2]^+$ the detailed mechanism remains elusive. However, it is proposed that the reaction is initiated by a ligand exchange wherein one of the chlorides of $[(TPA)Fe(III)Cl_2]^+$ is replaced by tert-butyl hydroperoxide (TBHP), see Figure 5.6. Based on the fact that a radical scavenger did not inhibit the reaction, the peroxide bond is proposed to be cleaved heterolytically (**path A**) [94]. This would result in a high valent iron(V)-oxo species. Following hydrogen atom abstraction from the substrate and radical recombination would then result in the chlorinated product.

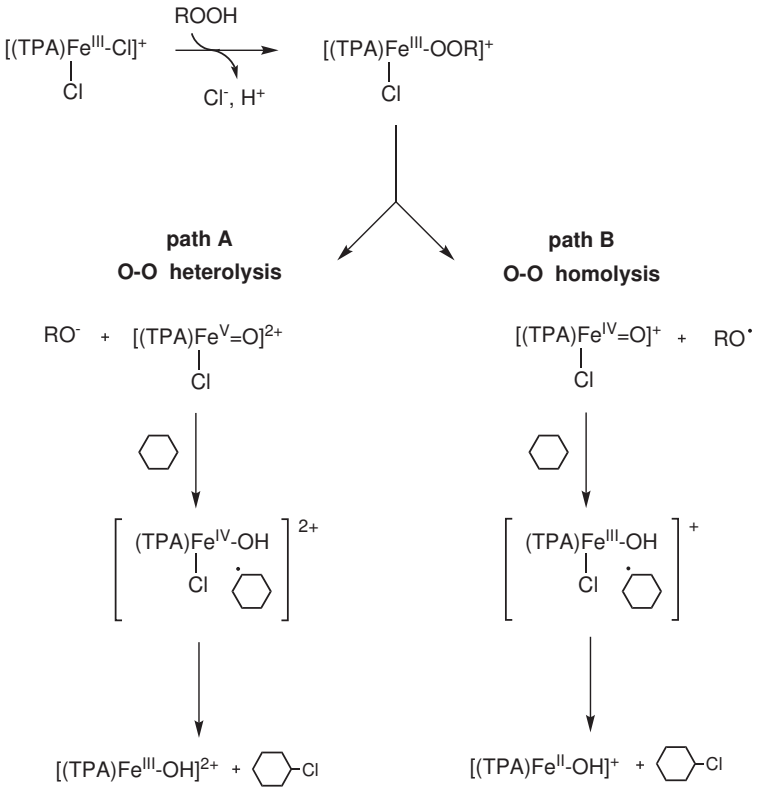

Figure 5.6: *Possible reaction paths for the oxidative halogenation of cyclohexane.*

However, even though the heterolytic bond cleavage of the peroxide is supported experimentally, a homolytic O-O bond cleavage can not be excluded (**path B**). In this case the result would be an iron(IV)-oxo species, an oxidation state of iron corresponding to the reactive species of the chlorinating enzyme SyrB2.

Introducing the oxidizing agent (ROOH) by a ligand-exchange reaction could lead to an axial (trans to the sp3 amine nitrogen) or equatorial (trans to an aromatic nitrogen) coordination. Thus, there are two possible isomers that might result from O-O bond heterolysis/homolysis, see Figure 5.7. The substrate cyclohexane can approach the complex from any direction, therefore both isomers exhibit similar behavior throughout the reaction course. Regarding the influence of the trans ligand, the N_{amine} complex is slightly more reactive than its $N_{aromatic}$ counterpart, and therefore only results for the N_{amine} complex will be presented here.

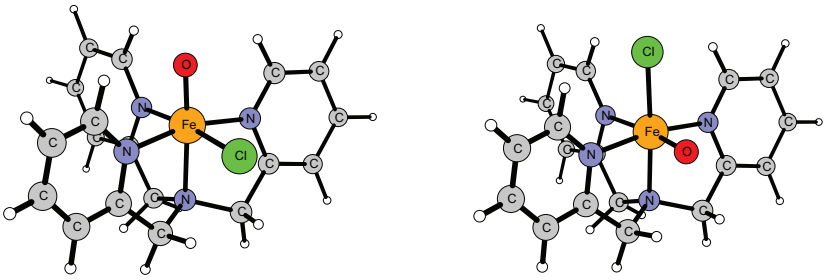

Figure 5.7: A: N_{amine} *complex with the oxo-group coordinating in the axial position trans to the sp3 amine nitrogen;* **B**: $N_{aromatic}$ *complex with the oxo-group coordinating the equatorial position trans to one of the aromatic nitrogen atoms.*

Iron(V)

The Cl-Fe(V)=O complex has a quartet ground state (S = 3/2). Calculations show that the unpaired spin density is mainly distributed within the iron-oxo unit. The calculated spin populations are 1.87 on the iron atom, 1.14 on the oxo atom and 0.05 on the chloride. This spin distribution can be explained with the molecular orbital picture describing the Fe(V)=O double bond, which is analogous to that of triplet dioxygen [95] (see the qualitative orbital picture in Figure 5.8). Two unpaired electrons each occupying a degenerate

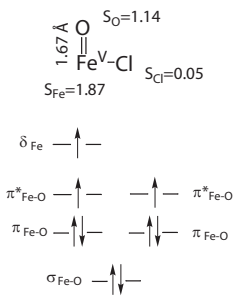

Figure 5.8: *Qualitative orbital picture describing the electronic structure of Cl-Fe^V=O.*

π^* orbital, yielding a spin population of about 1 on both, the iron center and the oxo group. The π^* electrons are ferromagnetically coupled to the remaining *d*-electron on the iron center, thus lowering the total energy by maximizing the exchange interaction.

According to the calculations, the reaction starts with an electron transfer from the substrate to the high-valent iron(V)-oxo species. In the resulting complex the cyclohexyl cation radical is attracted to the negatively charged chloride, see Figure 5.9. In this intermediate the iron atom can have either intermediate-spin ferromagnetically coupled to the unpaired electron on the substrate (M=4is), or high-spin antiferromagnetically coupled to the cyclohexyl cation (M=4hs). The high-spin complex is 2.9 kcal/mol higher than the intermediate-spin complex, see Figure 5.9.

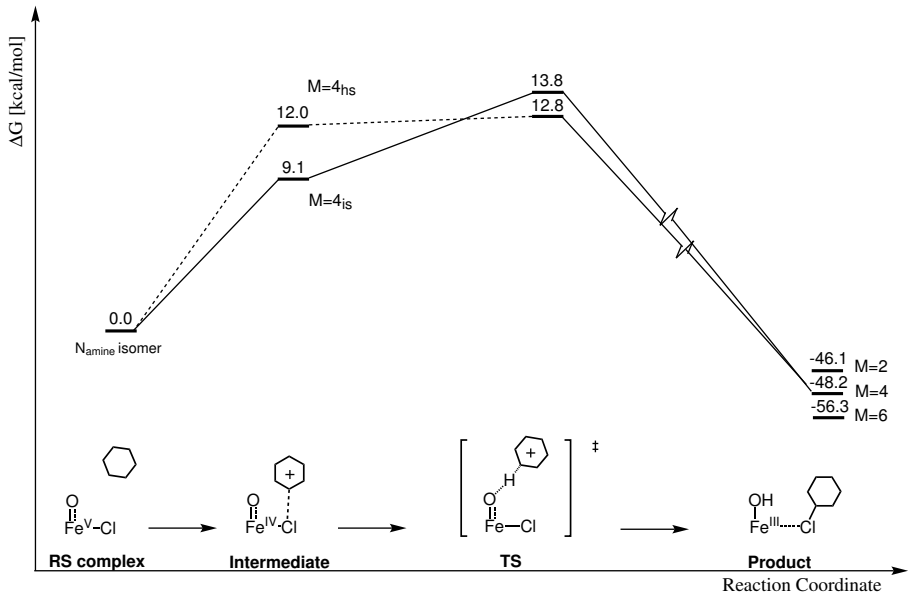

Figure 5.9: *Free-energy diagram for cyclohexane chlorination by* $[(TPA)ClFe(V)O]^{2+}$.

The reaction proceeds by a concerted mechanism in which hydrogen atom abstraction from the substrate leads directly to the chlorinated product. From the structure of the transition state it can be seen that this hydrogen atom abstraction occurs at an unusually long distance, which might be due to the repulsion between the cationic substrate and the positive charged complex (see Figure 5.10). The normal mode of this transition state is associated with elongation of the C-H bond and a bending vibration of the substrate within the plane spanned between the oxo group and the chloride. With the substrate bending towards the oxo-group its hydrogen atom is abstracted. Immediately after this the substrate is attracted to the negatively charged chloride which results in bond formation. The total barrier for this oxidative chlorination is only 12.8 kcal/mol for the high-spin species.

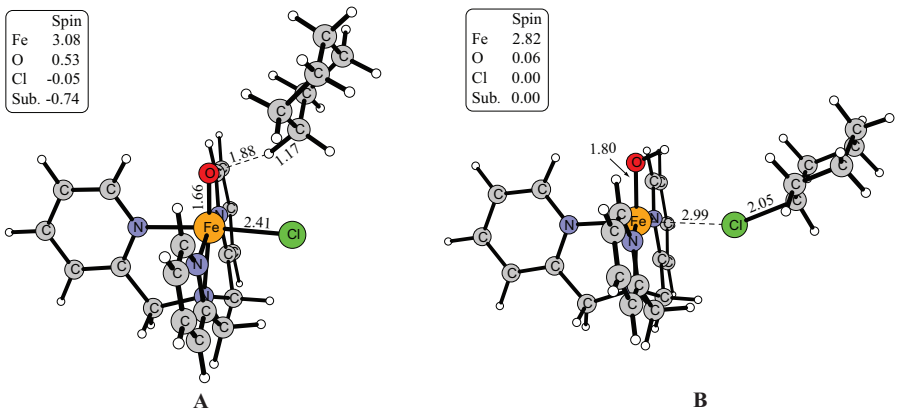

Figure 5.10: A: *The transition state for the concerted hydrogen atom abstraction and chloride rebound;* **B**: *The product of cyclohexane chlorination.*

The presented mechanism explains the exclusive chlorination observed for the $[(TPA)Fe(III)Cl_2]^+$ /TBHP system by a concerted hydrogen atom abstraction/chloride rebound step that leaves no time for the hydroxide to rotate and rebound to the substrate. However, the reaction is based on an ionic rather than on a radical mechanism as opposed the enzyme.

Iron(IV)

The calculated ground state of the Cl-Fe(IV)=O complex is characterized by one unpaired electron on the iron ion and one unpaired electron on the oxygen center, yielding a triplet multiplicity. This agrees with experimental data, where $[(TPA)ClFe(IV)O]^+$ was characterized as S=1 by a range of spectroscopic techniques [96]. However, the high-spin quintet state is only 4.4 kcal/mol higher, and therefore, the reaction with cyclohexane was investigated on both these potential-energy surfaces.

The hydrogen atom abstraction from the substrate has a barrier of 14.3 kcal/mol for the triplet state. In the resulting Fe(III)/cyclohexyl radical intermediate the unpaired electron of the substrate is ferromagnetically coupled to the low-spin iron center. On the quintet potential-energy surface two transition states for hydrogen atom abstraction have been found, leading to an intermediate with either high-spin or intermediate-spin on the iron ion. The hydrogen atom abstraction leading to the high-spin state (M=5hs) is 4.8 kcal/mol lower than the transition state on the triplet surface. Thus, starting from the reactant in its triplet ground state a spin crossing leading to high-spin state lowers the barrier for hydrogen atom abstraction from

14.3 to 9.5 kcal/mol, see Fig.5.11. After hydrogen atom abstraction an intermediate is formed, from which the reaction can proceed via chlorination or hydroxylation. For the high-spin state (M=5hs) the OH rebound occurs already at a distance of 2.87 Å with a barrier of only 3.4 kcal/mol. The barrier for the chlorine rebound is comparable but slightly higher with 5.1 kcal/mol. On the triplet surface these numbers are similar, that is 6.4 kcal/mol for hydroxo rebound and is 5.1 kcal/mol for chlorination.

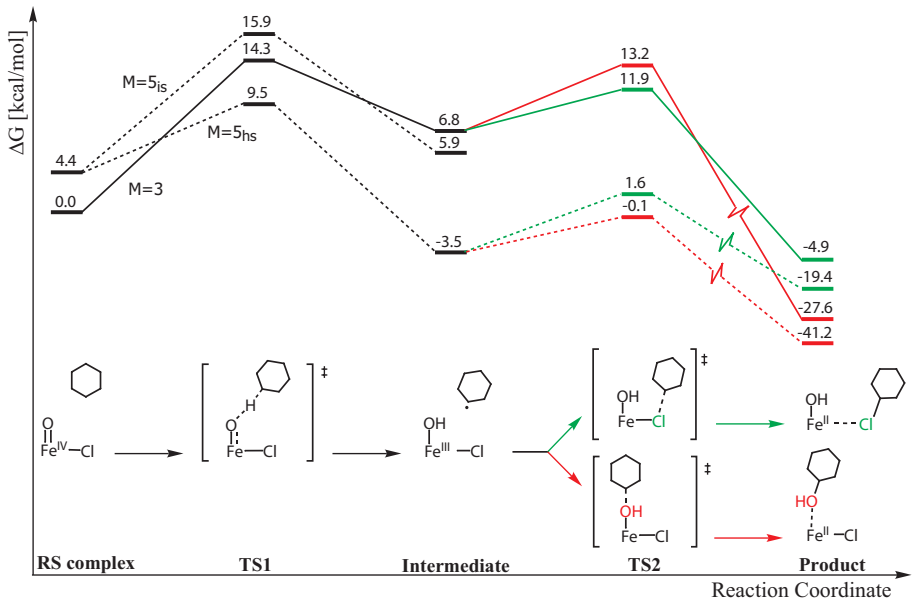

Figure 5.11: *Energy profile for hydrogen atom abstraction and radical rebound along the triplet and quintet potential-energy surfaces of $[(TPA)ClFe(IV)O]^{+}$.*

This means that the biomimetic Cl-Fe(IV)O complex would not be able to perform selective chlorination, since for the reactive high-spin state hydroxylation is slightly favored.

5.5 Conclusions

The results presented in this chapter clearly show how the enzyme is capable of selective chlorination, whereas the corresponding biomimetic iron(IV)-oxo complex is not able to discriminate between hydroxylation and chlorination.

For the enzyme it was shown that two ClFe(IV)=O isomers are reactive and decay to ClFe(III)(OH)/carbon radical intermediates via C-H bond

cleavage. The SyrB2 substrate binds in proximity to the coordination site where the oxo ligand is presumably formed. Once the oxoferryl intermediate is formed, the atomic ligands, i.e. oxo and chloro, easily exchange their binding sites leading to an equilibrium between the two oxoferryl species, as predicted by Mössbauer experiments [88, 90]. The following C-H cleavage step can in principle proceed with the engagement of either of the two species, and in the final rebound step, it is the ligand closest to the carbon radical, i.e. axial position *trans* to His235, which is preferentially rebounding to the carbon radical. For the native substrate (L-Thr) the lowest barrier for C-H cleavage was found for an isomer of the oxoferryl species favoring chlorination in the rebound step. Thus, the rate determining C-H cleavage step is decisive for the chemoselectivity of the reaction.

For the biomimetic iron complex the experimentally observed chlorination can only be explained by the presence of a high-valent iron(V) species. The high electron affinity of this complex leads to an early oxidation of the substrate. The following transition state for hydrogen atom abstraction is concerted and leads directly to the chlorinated product. The mechanism is different for the iron(IV)-oxo species, the oxidation state of iron also present in the enzyme. Here hydrogen atom abstraction leads to an intermediate, from which the barriers for hydroxylation/chlorination have similar heights, with a slight preference for hydroxylation.

6

Reactivity of a Binuclear Iron Complex

In this chapter a highly reactive iron dimer is presented. This complex has been synthesized by an experimental research group from Minnesota and resembles structural similarity to the active site of enzymes like MMO and RNR. The mechanism of dioxygen activation and substrate oxidation of these enzymes has already been discussed in chapter 2. It has been shown that dioxygen binds to the active site in between the two iron centers and forms two μ-oxo bridges upon O-O bond cleavage, resulting in a so-called diamond core[1]. The biomimetic complex presented here also has such diamond core, and in cooperation with the experimental group computations have been performed to investigate the reactivity of this structural unit.

6.1 Introduction

The biomimetic binuclear iron complex constitutes the first synthetic model complex with an iron(III)-iron(IV)-(μ-O)$_2$ core. It provides thus as an unique basis to investigate the reactivity of this structural motif outside the enzymatic environment. Interestingly, this complex shows a rather low reactivity for substrate oxidation in anhydrous acetonitrile. Only oxidation of weak C-H bonds is fast enough to be distinguished from self-decay. Experiments on the oxidation of the substrate dihydroanthracene (BDE = 78 kcal/mol) found that the reaction rate linearly increases as a function of water concentration, changing almost 200-fold from 0 to 1 M added water,

[1]The trapezoid resulting from this coordination looks like the shape of a diamond in a deck of cards and has, therefore, received this name.

see Figure 6.1. This observed rate enhancement corresponds to a free energy difference of about 3 kcal/mol.

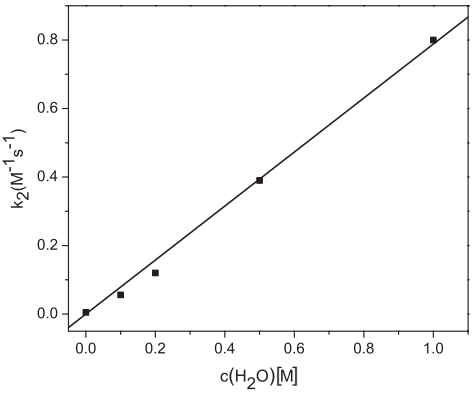

Figure 6.1: *Second order rate constants for the oxidation of dihydroanthracene by [Fe(III)Fe(IV)(μ-O)$_2$] in acetonitrile under argon at -30°C.*

A comparison of different iron(IV)-oxo units with the same supporting ligand (TPA) has shown, that the reactivity increases in the order $[Fe(III)Fe(IV)(\mu\text{-}O)_2]^{3+}$ < $[Fe(IV)_2(\mu\text{-}O)_2]^{4+}$ ≪ $[Fe(IV)=O]^{2+}$ [97]. This reactivity progression led credence to the proposal of water binding to the diamond core, thereby converting it into an "open-core" structure with one terminal iron(IV)-oxo group. The theoretical investigation on the reactivity of the diamond core is exemplified by hydroxylation of the substrate cyclohexane. The aim is to compare the reactivity of the diamond core with the hypothetical open core analogue, to draw conclusions about the catalytic active species (see Figure 6.2).

6.2 The Diamond Core

For the bis(μ-oxo) iron complex, B3LYP calculations predict a ground state in which the two high-spin iron centers are coupled antiferromagnetically, i.e. a doublet state $5\alpha4\beta$. In contrast, Mössbauer experiments predict a doublet ground state, resulting from ferromagnetic coupling between low-spin iron(III) and low-spin iron(IV) [54]. Obtaining the correct ground state for this type of complex is a difficult task computationally and depends on the admixture of exact exchange in the used density functional. If the amount of exact Hartree-Fock exchange is lowered below 10% the experimentally predicted ground state is obtained. However, the essential finding is that

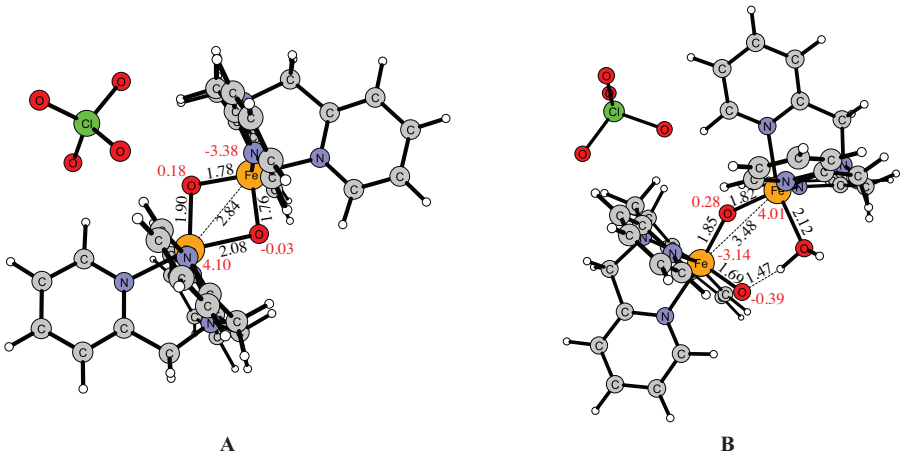

Figure 6.2: **A**: *The diamond core;* **B**: *The open core analogue. The non-coordinating* ClO_4^- *counter ion was included in the computational model complex. Red numbers indicate the spin on the iron and oxygen centers, respectively.*

a spin crossing to the reactive $5\alpha 4\beta$ doublet state occurs before the initial hydrogen atom abstraction. Figure 6.3 shows the calculated energy profile for the hydroxylation of cyclohexane. The barrier for hydrogen atom abstraction by the diamond core amounts to 22.0 kcal/mol. This relatively high barrier explains the low reactivity of this complex observed experimentally. The subsequent transition state for hydroxylation has a similar barrier with 21.8 kcal/mol in respect to the radical intermediate.

6.3 The Open-Core Analogue

When a water molecule coordinates to the iron(III) center of the diamond core, one of the two bridging μ-oxo groups is released from iron(III) and becomes a terminal oxo group on iron(IV). For this open core analogue calculations predict the same ground state as for the diamond core, i.e. a $5\alpha 4\beta$ doublet state resulting from antiferromagnetic coupling between the two high-spin irons. As can be seen in Figure 6.4, the barrier for hydrogen atom abstraction for this complex is only 15.0 kcal/mol. The predicted spin state of the intermediate complex formed after hydrogen atom abstraction is a singlet, $5\alpha 5\beta$, which is in perfect agreement with experiment [98]. Again, the hydroxylation step is comparable to the hydrogen atom abstraction with a barrier of 14.6 kcal/mol.

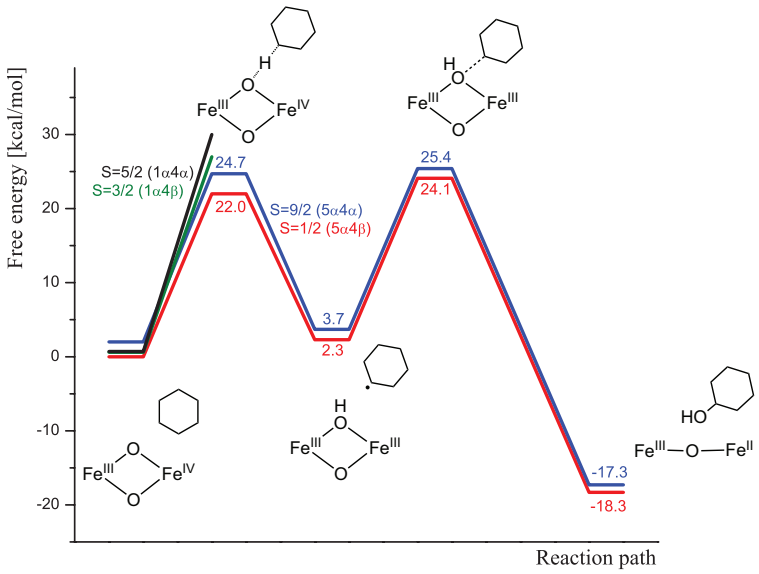

Figure 6.3: *Gibbs free energy profile for the hydroxylation of cyclohexane by the* $[Fe(III)Fe(IV)(\mu\text{-}O)_2]^{3+}$ *diamond core.*

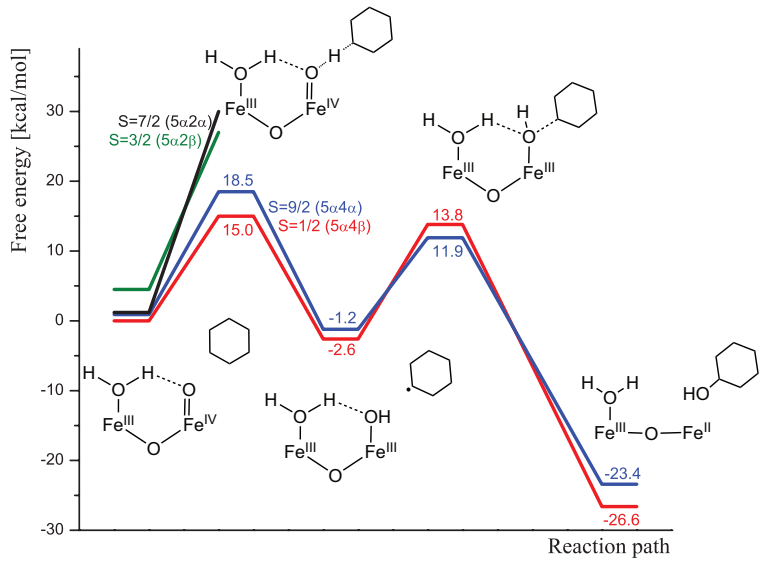

Figure 6.4: *Gibbs free energy profile for the hydroxylation of cyclohexane by the open core analogue* $[(H_2O)Fe(III)(\mu\text{-}O)Fe(IV)(O)]^{3+}$.

6.4 Conclusions

The computations predict that the hydrogen atom abstraction from cyclohexane has a lower barrier by 7.0 kcal/mol, when the oxidant has a terminal oxo group. This qualitative agreement with the experimental finding supports the proposed addition of water to the diamond core, upon which the complex opens up to form an iron(III)(OH)-(O)-iron(IV)(O) complex. The transition states for hydrogen atom abstraction are shown in Figure 6.5. It can be seen that for the open core analogue, the hydrogen

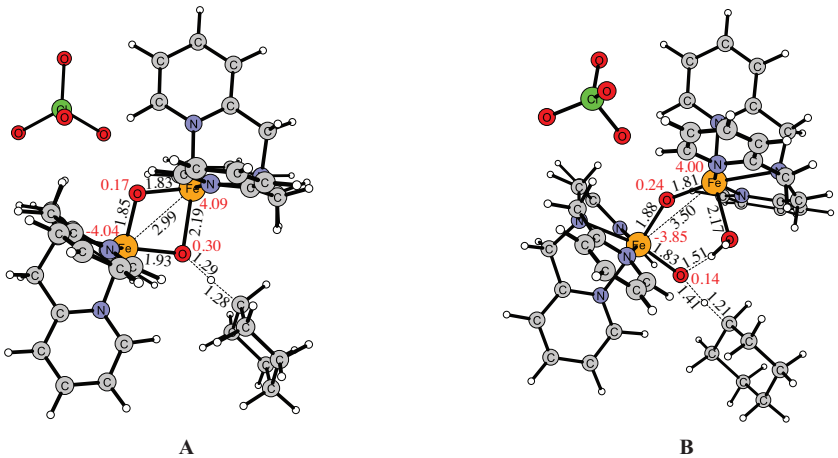

Figure 6.5: *Transition states for hydrogen atom abstraction* **A***: by the diamond core and* **B***: by its open core analogue.*

atom abstraction occurs quite early at 1.41 Å as compared to 1.29 Å for the diamond core. This different reactivity is explained by the fact that the terminal oxo group of the iron(IV)-oxo reactant (Figure 6.2) complex exhibits a more negative spin density (-0.39) than the two bridging oxo groups of the diamond core (0.18 and -0.03).

However, the computational approach overestimates the difference in reactivity somewhat. One possible explanation for this discrepancy could be that the binding of water is slightly endergonic, which would decrease the computed effect of water addition. This is supported by the fact that the intense green chromophore of the diamond core is persisting in the presence of water, and starts disappearing only during substrate oxidation. A second possibility could be that there were some traces of water in the solvent before the water addition, which would decrease the measured rate enhancement.

Sammanfattning på Svenska

Biomimetisk kemi är inriktad på simulering av enzymatisk reaktivitet, med hjälp av syntetiska analoger. I den här avhandlingen används kvantkemiska metoder för att studera mekanismer hos högreaktiva järnkomplex, som är involverade i inkorporering av syre eller klor i organiska molekyler. Den här typen av forskning syftar till att öka kunskapen om järnkomplexens reaktivitet.

I det första kapitlet beskrivs de teoretiska metoder som används i avhandlingen, som till exempel täthetsfunktionalteori och övergångstillståndsteori. Det andra kapitlet tar upp bakgrunden till järnets biologiska och syntetiska kemi. I resterande kapitel presenteras resultaten från de olika projekten som ingår i avhandlingen.

En av reaktionerna som studerats är omvandlingen av cyklohexan till adipinsyra (en viktig kemikalie i industriell kemi) katalyserad av ett järn(II)-porfyrinkomplex i närvaro av syrgas. Processen utgör ett 'grönt' alternativ till den konventionella produktionen av adipinsyra och är därför av stort intresse inom syntetisk kemi.

Klyvningen av en intradiol C-C bindning i katekol, katalyserad av ett järn(II)-komplex, är temat i det fjärde kapitlet. Det förklaras varför komplexet selektivt klyver intradiolbindingen och inte motsvarande extradiolbinding i katekol. Detta är en viktig fråga för förståelse av enzymatisk aktivitet.

Vidare har selektiv klorering i en nyupptäckt grupp av ickehem-järnenzymer studerats. Med hjälp av teoretisk modellering var det möjligt att föreslå en mekanism som förklarar observerad selektivitet. Dessutom påvisas hur ett biomimetisk järnkomplex simulerar den enzymatiska reaktiviteten, fast med en annan mekanism.

Ytterligare ett ämne som behandlas i den här avhandlingen är förhållandet mellan struktur och reaktivitet i ett binukleart järnkomplex, som har strukturell likhet med enzymer som t.ex. metanmonooxygenas och ribonunkleotidreduktas. Det påvisas vilken som är den aktiva form av komplexet, som reagerar med organiska molekyler.

References

[1] Roothaan C.J.J. New Developments in Molecular Orbital Theory. *Rev Mod Phys* **23**:69–89 (1951).

[2] Hall G.G. The molecular orbital theory of chemical valency VIII. A method of calculating ionization potentials. *Proc R Soc A* **205**:541–552 (1951).

[3] Moore W.J., Hummel D.O. Physikalische Chemie. *Walter de Gruyter* **4th ed.** (1986).

[4] Hohenberg P., Kohn W. Inhomogeneous Electron Gas. *Phys Rev B* **136**:864–871 (1964).

[5] Ceperley D.M., Alder B.J. Ground State of the Electron Gas by a Stochastic Method. *Phys Rev Lett* **45**:566–569 (1980).

[6] Vosko S., Wilk L., Nusair M. Accurate spin-dependent electron liquid correlation energies for local spin density calculations: a critical analysis. *Can J Phys* **58**:1200–1211 (1980).

[7] Becke A.D. Density-functional exchange-energy approximation with correct asymptotic behavior. *Phys Rev A* **38**:3098–3100 (1988).

[8] Perdew J. Density-functional approximation for the correlation energy of the inhomogeneous electron gas. *Phys Rev B* **33**:8822–8824 (1986).

[9] Lee C., Yang W., Parr R.G. Development of the Colle-Salvetti correlation-energy formula into a functional of the electron density. *Phys Rev B* **37**:785–789 (1988).

[10] Koch W., Holthausen M.C. A Chemist's Guide to Density Functional Theoryâ. *Wiley-VCH Verlag GmbH* **2nd ed.** (2001).

[11] Harris J. Adiabatic-connection approach to Kohn-Sham theory. *Phys Rev A* **29**:1648–1659 (1984).

[12] Becke A.D. A new mixing of Hartree-Fock and local density-functional theories. *J Chem Phys* **98**:1372–1377 (1993).

[13] Ruiz E., Salahub D.R., Vela A. Charge-Transfer Complexes: Stringent Tests for Widely Used Density Functionals. *J Phys Chem* **100**:12265–12276 (1996).

[14] Sodupe M., Bertran J., Rodriguez-Santiago L., Baerends E.J. Ground State of the (H2O)2+ Radical Cation: DFT versus Post-HartreeâFock Methods. *J Phys Chem A* **103**:166–170 (1999).

REFERENCES

[15] Lundberg M., Siegbahn P.E.M. Quantifying the effects of the self-interaction error in DFT: When do the delocalized states appear? *J Chem Phys* **122**:24103:1–9 (2005).

[16] Vydrov O.A., Scuseria G.E. Effect of the Perdew–Zunger self-interaction correction on the thermochemical performance of approximate density functionals. *J Chem Phys* **121**:8187–8193 (2004).

[17] Polo V., Kraka E., Cremer D. Electron correlation and the self-interaction error of density functional theory. *Mol Phys* **100**:1771–1790 (2002).

[18] Allen M.J., Tozer D.J. Helium dimer dispersion forces and correlation potentials in density functional theory. *J Chem Phys* **117**:11113–11120 (2002).

[19] Zimmerli U., Parrinello M., Koumoutsakos P. Dispersion corrections to density functionals for water aromatic interactions. *J Chem Phys* **120**:2693–2699 (2004).

[20] Grimme S. Accurate Description of van der Waals Complexes by Density Functional Theory Including Empirical Corrections. *J Comp Chem* **25**:1463–1473 (2004).

[21] Grimme S. Semiempirical GGA-Type Density Functional Constructed with a Long-Range Dispersion Correction. *J Comp Chem* **27**:1787–1799 (2006).

[22] Noodleman L. Valence bond description of antiferromagnetic coupling in transition metal dimers. *J Chem Phys* **74**:5737–5743 (1981).

[23] Noodleman L., Case D.A. Density-Functional Theory Of Spin Polarization And Spin Coupling In Iron-Sulfur Clusters. *Adv Inorg Chem* **38**:423–458 (1992).

[24] Curtiss L.A., Redfern P., Raghavachari K. Assessment of Gaussian-3 and density-functional theories on the G3/05 test set of experimental energies. *J Chem Phys* **123**:124107:1–12 (2005).

[25] Blomberg, Siegbahn P.E.M., Svensson M. Comparisons of results from parametrized configuration interaction (PCI-80) and from hybrid density functional theory with experiments for first row transition metal compounds. *J Chem Phys* **104**:9546–9554 (1996).

[26] Ricca A., Bauschlicher C.W. Successive OH Binding Energies of M(OH)n+ for n=1-3 and M=Sc, Ti, V, Co, Ni, and Cu. *J Phys Chem A* **101**:8949–8955 (1997).

[27] Ricca A., Bauschlicher C.W. Successive binding energies of Fe(CO)5+. *J Phys Chem* **98**:12899–12903 (1994).

[28] Siegbahn P.E.M., Blomberg M. Transition-Metal Systems in Biochemistry Studied by High-Accuracy Quantum Chemical Methods. *Chem Rev* **100**:421–438 (2000).

[29] Schröder D., Shaik S., Schwarz H. Two-State Reactivity as a New Concept in Organometallic Chemistry. *Acc Chem Res* **33**:139–146 (2000).

[30] Danovich D., Shaik S. Spin-Orbit Coupling in the Oxidative Activation of H-H by FeO+. Selection Rules and Reactivity Effects. *J Am Chem Soc* **119**:1773–1786 (1997).

[31] Cox P.A. The elements: their origin, abundance, and distributionâ. *Oxford University Press* **2nd ed.** (1997).

[32] Küster F.W., Thiel A. Rechentafeln für die chemische Analytik. *Walter de Gruyter* (1993).

[33] Pearson R.G. Acid and Bases. *Science* **151**:172–177 (1966).

[34] Mann S., Webb J., Williams R.J.P. Biomineralization: chemical and biochemical perspectives. *VCH-Weinheim* (1989).

[35] Jensen K., Ryde U. How O2 Binds to Heme: Reasons For Rapid Binding And Spin Inversion. *J Biol Chem* **279**:14561–14569 (2004).

[36] Harris D.L., Loew G.H. Theoretical Investigation of the Proton Assisted Pathway to Formation of Cytochrome P450 Compound I. *J Am Chem Soc* **120**:8941–8948 (1998).

[37] Que L. One motif-many different reactions. *Nat Struct Biol* **7**:182–184 (2000).

[38] Koehntop K.D., Emerson J.P., Que L. The 2-His-1-carboxylate facial triad: a versatile platform for dioxygen activation by mononuclear non-heme iron(II) enzymes. *JBIC* **10**:87–93 (2005).

[39] Solomon E.I., Brunold T.C., Davis M.I., Kemsley J.N., Lee S.K., Lehnert N., Neese F., Skulan A.J., Yang Y.S., Zhou J. Geometric and Electronic Structure/Function Correlations in Non-Heme Iron Enzymes. *Chem Rev* **100**:235–350 (2000).

[40] Price J.C., Barr E.W., Tirupati B., Bollinger J.M., Krebs C. The First Direct Characterization of a High-Valent Iron Intermediate in the Reaction of an a-Ketoglutarate-Dependent Dioxygenase: A High-Spin Fe(IV) Complex in Taurine/a-Ketoglutarate Dioxygenase (TauD) from Escherichia coli. *Biochem* **43**:1134 (2004).

[41] Bassan A., Borowski T., Siegbahn P.E.M. Quantum chemical studies of dioxygen activation by mononuclear non-heme iron enzymes with the 2-His-1-carboxylate facial triad. *Dalton Trans* **2004**:3153–3162 (2004).

[42] Blasiak L.C., Vaillancourt F.H., Walsh C.T., Drennan C.L. Crystal structure of the non-haem iron halogenase SyrB2 in syringomycin biosynthesis. *Nature* **440**:368–371 (2006).

[43] Matthews M.L., Neumann C.S., Miles L.A., Grove T.L., Booker S.J., Krebs C., Walsh C.T., Bollinger J.M. Substrate positioning controls the partition between halogenation and hydroxylation in the aliphatic halogenase, SyrB2. *PNAS* **106**:17723–17728 (2009).

[44] Wilkins R.G. Binuclear iron centres in proteins. *Chem Soc Rev* **21**:171–178 (1992).

[45] Lipscomb J.D., Que L. MMO: P450 in wolf's clothing? *JBIC* **3**:331–336 (1998).

[46] Brazeau B.J., Lipscomb J.D. Kinetics and Activation Thermodynamics of Methane Monooxygenase Compound Q Formation and Reaction with Substrates. *Biochem* **39**:13503–13515 (2000).

REFERENCES

[47] Tshuva E.Y., Lippard S. Synthetic Models for Non-Heme Carboxylate-Bridged Diiron Metalloproteins: Strategies and Tactics. *Chem Rev* **104**:987–1012 (2004).

[48] Kryatov S.V., Rybak-Akimova E.V., Schindler S. Kinetics and Mechanisms of Formation and Reactivity of Non-heme Iron Oxygen Intermediates. *Chem Rev* **105**:2175–2226 (2005).

[49] Kraatz H.B., Metzler-Nolte N. Concepts and models in bioinorganic chemistry. *VCH-Weinheim* **3rd ed** (2006).

[50] Shan X., Que L. High-valent nonheme iron-oxo species in biomimetic oxidations. *J Inorg Biochem* **100**:421–433 (2006).

[51] Zhou Y., Shan X., Mas-Ballesté R., Bukowski M.R., Stubna A., Chakrabarti M., Slominski L., Halfen J.A., Münck E., Que L. Contrasting cis and trans Effects on the Reactivity of Nonheme Oxoiron(IV) Complexes. *Angew Chem Int Ed* **47**:1896–1899 (2008).

[52] Decker A., Solomon E. Comparison of FeIV=O Heme and Non-heme Species: Electronic Structures, Bonding, and Reactivities. *Angew Chem Int Ed* **44**:2252–2255 (2005).

[53] Hirao H., Que L., Kumar D., Shaik S. Two-State Reactivity in Alkane Hydroxylation by Non-Heme Iron-Oxo Complexes. *J Am Chem Soc* **128**:8590–8606 (2006).

[54] Que L., Tolman W.B. Bis(m-oxo)dimetal "Diamond" Cores in Copper and Iron Complexes Relevant to Biocatalysis. *Angew Chem Int Ed* **41**:1114–1137 (2002).

[55] Zang Y., Dong Y., Que L., Kauffmann K., Münck E. The First Bis(m-oxo)diiron(III)Complex. Structure and Magnetic Properties of [Fe2(m-O)2(6TLA)2](ClO4)2. *J Am Chem Soc* **117**:1169–1170 (1995).

[56] Zang Y., Pan G., Que L., Fox B. First Diferric Complex with an Fe2(m-O)(m-OH) Core. Structure and Reactivity of [Fe2(m-O)(m-OH)(6TLA)2]l(ClO4)3. *J Am Chem Soc* **116**:3653–3654 (1994).

[57] Kroschwitz J.I., Kirk-Othmer. Kirk-Othmer Encyclopedia of Chemical Technology, A to Alkaloids. *John Wiley & Sons* **4th ed.** (1991).

[58] Iwahama T., Syojyo K., Sakaguchi S., Ishii Y. Direct Conversion of Cyclohexane into Adipic Acid with Molecular Oxygen Catalyzed by N-Hydroxyphthalimide Combined with Mn(acac)2 and Co(OAc)2. *Org Proc Res Dev* **2**:255–260 (1998).

[59] Pigamo A., Besson M., Blanc B., Gallezot P., Blackburn A., Kozynchenko O., Tennison S., Crezee E., Kapteijn F. Effect of oxygen functional groups on synthetic carbons on liquid phase oxidation of cyclohexanone. *Carbon* **40**:1267–1278 (2002).

[60] Raja R., Thomas J.M. Catalyst design strategies for controlling reactions in microporous and mesoporous molecular-sieves. *J Mol Cat A* **181**:3–14 (2002).

[61] Saji P., Ratnasamy C., Gopinathan S. Process for the oxidation of cyclohexane to adipic acid. *United States Patent* (2002).

[62] Yuan Y., Ji H., Chen Y., Han Y., Song X., She Y., Zhong R. Oxidation of Cyclohexane to Adipic Acid Using Fe-Porphyrin as a Biomimetic Catalyst. *Org Proc Res Dev* **8**:418–420 (2004).

[63] Chin D., Mar G.L., Balch A. Detection and Characterization of the Long-Postulated Fe-00-Fe Intermediate in the Autoxidation of Ferrous Porphyrins. *J Am Chem Soc* **99**:5486–5488 (1977).

[64] Chin D., Mar G.L., Balch A. On the Mechanism of Autoxidation of iron (II) porphyrins. Detection of a Peroxo-Bridged Iron (III) Porphyrin Dimer and the Mechanism of Its Thermal Decomposition to the Oxo-Bridged Iron (III) Porphyrin Dimer. *J Am Chem Soc* **102**:4344–4350 (1980).

[65] Balch A., Chan Y., Cheng R., Mar G.L., Latos-Grazynski L., Renner M.W. Oxygenation Patterns for iron(II) Porphyrins. Peroxo and Ferryl (FeIVO) Intermediates Detected by 1H Nuclear Magnetic Resonance Spectroscopy during the Oxygenation of (Tetramesitylporphyrin)iron(II). *J Am Chem Soc* **106**:7779–7785 (1984).

[66] Balch A. The reactivity of spectroscopically detected peroxy complexes of iron porphyrins. *Inorg chim ac* **198-200**:297–307 (1992).

[67] Ghiladi R.A., Kretzer R.M., Guzei I., Rheingold A.L., Neuhold Y.M., Hatwell K.R., Zuberbühler A.D., Karlin K.D. (F8TPP)FeII/O2 Reactivity Studies F8TPP=Tetrakis(2,6-difluorophenyl)porphyrinate(2-): Spectroscopic (UV-Visible and NMR) and Kinetic Study of Solvent-Dependent (Fe/O2 = 1:1 or 2:1) Reversible O2-Reduction and Ferryl Formation. *Inorg Chem* **40**:5754–5767 (2001).

[68] She Y. Private Communication. *Institute of Green Chemistry, Beijing University of Technology, Beijing, China* .

[69] Kovaleva E., Lipscomb J.D. Crystal Structures of Fe2+ Dioxygenase Superoxo, Alkylperoxo, and Bound Product Intermediates. *Science* **316**:453–457 (2007).

[70] Kovaleva E.G., Neibergall M.B., Chakrabarty S., Lipscomb J.D. Finding intermediates in the O2 activation pathways of non-heme iron oxygenases. *Acc Chem Res* **40**:475–483 (2007).

[71] Siegbahn P.E.M., Haeffner F. Mechanism for Catechol Ring-Cleavage by Non-Heme Iron Extradiol Dioxygenases. *J Am Chem Soc* **126**:8919–8932 (2004).

[72] Huisgen R., Gilde H.G. Rudolf Criegee (1902-1975). *J Chem Educ* **56**:369 (1979).

[73] Borowski T., Georgiev V., Siegbahn P.E.M. Catalytic Reaction Mechanism of Homogentisate Dioxygenase: A Hybrid DFT Study. *J Am Chem Soc* **127**:17303–17314 (2005).

[74] Georgiev V., Borowski T., Blomberg M., Siegbahn P.E.M. A comparison of the reaction mechanisms of iron- and manganese-containing 2,3-HPCD: an important spin transition for manganese. *JBIC* **13**:929–940 (2008).

[75] Borowski T., Siegbahn P.E.M. Mechanism for Catechol Ring Cleavage by Non-Heme Iron Intradiol Dioxygenases: A Hybrid DFT Study. *J Am Chem Soc* **128**:12941–12953 (2006).

[76] Cox D., Que L. Functional Models for Catechol 1,2-Dioxygenase. The Role of the Iron(III) Center. *J Am Chem Soc* **110**:8085–8092 (1988).

[77] Bruijnincx P., Lutz M., Spek A., Hagen W., van Koten G., Klein-Gebbink R.J.M. Iron(III)-Catecholato Complexes as Structural and Functional Models of the Intradiol-Cleaving Catechol Dioxygenases. *Inorg Chem* **46**:8391–8402 (2007).

[78] Koch W., Krüger H. Ein sehr reaktives und katalytisch wirksames Modellsystem für intradiolspaltende Catechol-Dioxygenasen: Struktur und Reaktivitat von Eisen(m)-Catecholatkomplexen von N,N′-Dimethyl-2,11-diaza[3.3](2,6)pyridinophan. *Angew Chem* **107**:2928–2931 (1995).

[79] Walsh T., Ballou D., Mayer R., Que L. Rapid ReactionStudieson the Oxygenation Reactionsof Catechol Dioxygenase. *J Biol Chem* **258**:14422–14427 (1983).

[80] Georgiev V., Borowski T., Siegbahn P.E.M. Theoretical study of the catalytic reaction mechanism of MndD. *JBIC* **11**:571–585 (2006).

[81] Xin M., Bugg T.D.H. Evidence from Mechanistic Probes for Distinct Hydroperoxide Rearrangement Mechanisms in the Intradiol and Extradiol Catechol Dioxygenases. *J Am Chem Soc* **130**:10422–10430 (2008).

[82] Groce S., Lipscomb J.D. Conversion of Extradiol Aromatic Ring-Cleaving Homoprotocatechuate 2,3-Dioxygenase into an Intradiol Cleaving Enzyme. *J Am Chem Soc* **125**:11780–11781 (2003).

[83] Vaillancourt F., Yeh E., Vosburg D., Gameau-Tsodikova S., Walsh C.T. Nature's Inventory of Halogenation Catalysts: Oxidative Strategies Predominate. *Chem Rev* **106**:3364–3378 (2006).

[84] Vaillancourt F., Yin J., Walsh C. SyrB2 in syringomycin E biosynthesis is a nonheme FeII a-ketoglutarate-and O2-dependent halogenase. *PNAS* **102**:10111–10116 (2005).

[85] Schnarr N.A., Khosla C. Just add chlorine. *Nature* **436**:1094–1095 (2005).

[86] Hausinger R. Fe(II)/a-Ketoglutarate-Dependent Hydroxylases and Related Enzymes. *Crit Rev Biochem Mol Biol* **39**:21–68 (2004).

[87] Borowski T., Bassan A., Siegbahn P.E.M. Mechanism of Dioxygen Activation in 2-Oxoglutarate-Dependent Enzymes: A Hybrid DFT Study. *Chem Eur J* **10**:1031–1041 (2004).

[88] Galonic D.P., Barr E.W., Walsh C.T., Bollinger J.M., Krebs C. Two interconverting Fe(IV) intermediates in aliphatic chlorination by the halogenase CytC3. *Nat Chem Biol* **3**:113–116 (2007).

[89] Fujimori D.G., Barr E.W., Matthews M., Koch G., Yonce J.R., Walsh C.T., Bollinger J.M., Krebs C., Riggs-Gelasco P.J. Spectroscopic Evidence for a High-Spin Br-Fe(IV)-Oxo Intermediate in the a-Ketoglutarate-Dependent Halogenase CytC3 from Streptomyces. *J Am Chem Soc* **129**:13408–13409 (2007).

[90] Matthews M.L., Krest C.M., Barr E.W., Vaillancourt F.H., Walsh C.T., Green M.T., Krebs C., Bollinger J.M. Substrate-Triggered Formation and Remarkable Stability of the C-H Bond-Cleaving Chloroferryl Intermediate in the Aliphatic Halogenase, SyrB2. *Biochem* **48**:4331–4343 (2009).

[91] Zhou J., Kelly W.L., Bachmann B.O., Gunsior M., Townsend C.A., Solomon E.I. Spectroscopic Studies of Substrate Interactions with Clavaminate Synthase 2, a Multifunctional R-KG-Dependent Non-Heme Iron Enzyme: Correlation with Mechanisms and Reactivities. *J Am Chem Soc* **123**:7388–7398 (2010).

[92] Neidig M.L., Kavana M., Moran G.R., Solomon E.I. CD and MCD Studies of the Non-Heme Ferrous Active Site in (4-Hydroxyphenyl)pyruvate Dioxygenase: Correlation between Oxygen Activation in the Extradiol and a-KG-Dependent Dioxygenases. *J Am Chem Soc* **126**:4486–4487 (2010).

[93] Krebs C., Fujimori D.G., Walsh C.T., Bollinger J.M. Non-Heme Fe (IV)–Oxo Intermediates. *Acc Chem Res* **40**:484–492 (2007).

[94] Kojima T., Leising R.A., Yan S., Que L. Alkane Functionalization at Nonheme Iron Centers. Stoichiometric Transfer of Metal-Bound Ligands to Alkane. *J Am Chem Soc* **115**:11328–11335 (1993).

[95] Shaik S., Filatov M., Schröder D., Schwarz H. Electronic Structure Makes a Difference: Cytochrome P-450 Mediated Hydroxylations of Hydrocarbons as a Two-State Reactivity Paradigm. *Chem Eur J* **4**:193–199 (1998).

[96] Rohde J.U., Stubna A., Bominaar E.L., Münck E., Nam W., Que L. Nonheme Oxoiron(IV) Complexes of Tris(2-pyridylmethyl)amine with cis-Monoanionic Ligands. *Inorg Chem* **45**:6435–6445 (2006).

[97] Xue G., Wang D., Hont R.D., Fiedler A.T., Shan X., Münck E., Que L. A synthetic precedent for the [FeIV2(m-O)2] diamond core proposed for methane monooxygenase intermediate Q. *PNAS* **104**:20713–20718 (2007).

[98] Dong Y., Fujii H., Hendrich M.P., Leising R.A., Pan G., Randall C.R., Wilkinson E.C., Zang Y., Que L., Fox B.G., Kauffmann K., Münck E. A High-Valent Nonheme Iron Intermediate. Structure and Properties of [Fe2(m-O)2(5-Me-TPA)2](ClO4)3. *J Am Chem Soc* **117**:2778–2792 (1995).